

RESEARCH ARTICLE | SEPTEMBER 17 2024

## Flow over two inline rough cylinders in the postcritical regime

Anil Pasam ; Daniel Tudball Smith ; David Burton ; Mark C. Thompson 



*Physics of Fluids* 36, 095145 (2024)

<https://doi.org/10.1063/5.0221390>



### Articles You May Be Interested In

Flow past a normal flat plate undergoing inline oscillations

*Physics of Fluids* (September 2012)

Effects of size ratio and inter-cylinder spacing on wake transition in flow past finite inline circular cylinders mounted on plane surface

*Physics of Fluids* (February 2021)

On the bi-stability of flow around two tandem circular cylinders at a subcritical Reynolds number of 3900

*Physics of Fluids* (October 2024)



## Physics of Fluids

Special Topic:

Recent Advances in Fluid Dynamics and its Applications

Guest Editors: B.Reddappa, B. Rushi Kumar, Sreedhara Rao Gunakala, Bijula Prabhakar Reddy

[Submit Today!](#)

# Flow over two inline rough cylinders in the postcritical regime

Cite as: Phys. Fluids **36**, 095145 (2024); doi: [10.1063/5.0221390](https://doi.org/10.1063/5.0221390)

Submitted: 31 May 2024 · Accepted: 30 August 2024 ·

Published Online: 17 September 2024



View Online



Export Citation



CrossMark

Anil Pasam,<sup>a)</sup> Daniel Tudball Smith, David Burton, and Mark C. Thompson

## AFFILIATIONS

Fluids Laboratory for Aeronautical and Industrial Engineering (FLAIR), Department of Mechanical and Aerospace Engineering, Monash University, Clayton VIC 3800, Australia

<sup>a)</sup> Author to whom correspondence should be addressed: [anil.pasam@monash.edu](mailto:anil.pasam@monash.edu)

## ABSTRACT

This study investigates the flow behavior over roughened inline cylinders for postcritical flow, a parameter space with relatively little prior scrutiny. Two cylinders of the same relative surface roughness,  $k_s/D = 1.9 \times 10^{-3}$ , separated by a pitch (i.e.,  $L$ , distance between the centers of two cylinders) between  $1.175 \leq L/D \leq 10$  are studied at Reynolds numbers from  $3 \times 10^5$  to  $6 \times 10^5$  using unsteady surface pressure measurements. As pitch ratio is increased from  $L/D = 1.175$ ,  $C_D$  of the downstream cylinder increases sharply at  $(L/D)_c = 3.25$ . This critical pitch ratio  $(L/D)_c$  is toward the lower end of the reported range for *subcritical smooth cylinders*. Asymmetric mean gap flow along with alternating reattachment is found for  $1.5 \leq L/D < 2.25$  (i.e., two asymmetric modes in the gap, mode 1 and mode 2, that are the reflections of each other), and symmetric gap flow with a continuous reattachment is found for  $2.25 < L/D \leq 3$ . The gap flow is also symmetric for the closest pitch ratio tested of  $L/D = 1.175$ . While the change in upstream cylinder drag coefficient with Reynolds number broadly follows that of an isolated cylinder, for the downstream cylinder, it is approximately independent. The critical separation is also insensitive to Reynolds number within  $3 \times 10^5 \leq Re \leq 6 \times 10^5$ . Transitions between the reattachment and the co-shedding flow are predominantly continuous over the spanwise planes tested. On the other hand, alternating reattachment occurs in spanwise cells, where one sectional measurement exhibits the asymmetric mode 1 while a spanwise-adjacent section exhibits the asymmetric mode 2 or even symmetric flow. Previously reported maxima in the fluctuating lift and drag coefficients of the downstream cylinder at  $L/D \approx 2.4$  at subcritical Reynolds numbers are absent in the current investigation.

© 2024 Author(s). All article content, except where otherwise noted, is licensed under a Creative Commons Attribution (CC BY) license (<https://creativecommons.org/licenses/by/4.0/>). <https://doi.org/10.1063/5.0221390>

## I. INTRODUCTION

Engineered structures such as heat exchangers, boilers, oil rigs, and chimneys are often constructed from cylindrical or near cylindrical components with circular cross sections. In many cases, such cylindrical structures are under the aerodynamic influence of other structures nearby. This study focuses on a common arrangement, one circular cylinder directly downstream of another, subject to varying spacing, in an attempt to understand the complex aerodynamic interactions between the two cylinders and the resulting forces on each component. For the remainder of the paper, we refer to this arrangement as the *inline* configuration. An investigation of the inline arrangement serves as a foundation for the analysis of the more general arrangement, where the two cylinders are separated in both streamwise and cross-stream directions.

Within the context of flow over single cylinders, four flow regimes: subcritical, critical, supercritical, and postcritical, have been

identified based on the behavior of the flow and forces as the Reynolds number is increased. For the highest-Reynolds-number postcritical regime, which is the focus of this study, the transition to turbulence in the cylinder boundary layer occurs sufficiently far upstream that the influence of further increases in Reynolds number is only minor (Roshko, 1961).

Atmospheric flows over man-made structures are often postcritical owing to large diameters, high turbulence, high peak wind speeds, and surface roughness due to imperfections caused by paint, weathering, surface texture, corrosion, etc. The current work is aimed at understanding this particular flow scenario, i.e., *flow over two rough inline cylinders in the postcritical regime*.

Zdravkovich (1977), Sumner (2010), and Zhou and Alam (2016) have reviewed experimental investigations involving the flow over two cylinders in various arrangements subject to different Reynolds numbers. With the exception of Okajima (1979), Zdravkovich (1980), and

Dubois and Andrianne (2022), the majority of the previous works on inline cylinders have focused on smooth cylinders. In addition, only a select few (e.g., Okajima, 1979; Schewe and Jacobs, 2019; Schewe *et al.*, 2021; and Dubois and Andrianne, 2022) have examined postcritical Reynolds numbers.

Although roughness decreases the critical Reynolds number for the occurrence of the drag crisis and increases the postcritical drag coefficient, the flow over rough cylinders in the postcritical regime is similar to that occurring over smooth cylinders. They both experience periodic vortex shedding, a wider wake, and a similar dependence on the changes in Reynolds number (Roshko, 1961; van Hinsberg, 2015; and Pasam *et al.*, 2023). Thus, two rough inline cylinders in the postcritical regime may be expected to show similarities in behavior to two smooth cylinders in the subcritical regime, at least in a qualitative sense. Hence, we consider the features of the flow over inline smooth cylinders to provide a baseline for comparison.

In the current investigation, cylinder spacing is represented using the non-dimensional pitch ratio,  $L^* = L/D$ , where  $L$  is the distance between the centers of the two cylinders and  $D$  is the diameter of each cylinder (see Fig. 2). For inline cylinder flow, Zdravkovich (1987) classified the flow topology into three different patterns that are consequences of pitch ratio and incoming flow properties. Other investigators have put forward different classification schemes. As many as eight flow configurations were identified in Igarashi (1984) in  $2.5 \times 10^4 \leq Re \leq 6.4 \times 10^4$  based on the intermittent flow structure in the gap between the cylinder, and more recently, Zhou and Yiu (2006) proposed a classification with four regimes. The current investigation uses the nomenclature of the three regimes from Zdravkovich (1987), which are illustrated in Fig. 1 and described as follows:

1. The **extended body regime** is observed at very small pitch ratios. In this regime, the separated shear layers from the upstream cylinder envelop the downstream cylinder forming only one vortex street from each side of the cylinders. The two cylinders thus act as a single bluff body, i.e. an “extended body.” This regime spans  $1 < L^* \leq 2$  at  $Re \approx 10^4$ , and the upper bound rapidly decreases with increasing Reynolds number (Igarashi, 1981; 1984).
2. The **reattachment regime** is when the downstream cylinder is placed such that the shear layers from the upstream cylinder reattach onto the downstream cylinder. For  $Re = 7000$ , Zhou and

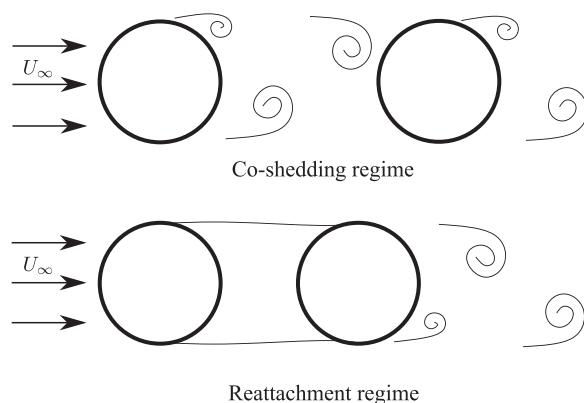


FIG. 1. Schematic of the representative flow structure in the co-shedding and the reattachment regimes.

Yiu (2006) found that shear layers reattach on the downstream side ( $90^\circ \leq \theta \leq 180^\circ$ , where  $\theta$  is the azimuthal angle, see Fig. 2) on the downstream cylinder at  $L^* = 2.5$  while they reattach on the upstream side ( $0^\circ \leq \theta \leq 90^\circ$ ) for  $L^* = 4$ . At larger Reynolds numbers, Zdravkovich (1977) and Alam *et al.* (2003) reported a mean reattachment angle (based on circumferential pressure distributions) on the forward surface ( $0^\circ \leq \theta \leq 90^\circ$ ) of the downstream cylinder for all reattachment pitch ratios. Alam *et al.* (2003) further classified the reattachment regime into alternating and steady reattachment at  $1 < L^* < 3$  and  $3 < L^* < 4$ , respectively.

3. The **co-shedding regime** is observed when the downstream cylinder is sufficiently downstream that the separated shear layers from the upstream cylinder roll up before reaching it. In this regime, Kármán vortex shedding is observed from both the cylinders. This regime is observed for  $L^* > \approx 4$ .

The boundaries between the different regimes depend on the incoming Reynolds number (Sumner, 2010; Igarashi, 1981), the incident turbulence intensity (Ljungkrona *et al.*, 1991), and the surface roughness (Dubois and Andrianne, 2022).

The pitch ratio at which the flow state changes from a predominantly reattachment regime to a predominantly co-shedding regime is known as the critical pitch ratio,  $L_c^*$ , and it lies in between  $L^* = 3$ –5 depending on Reynolds number (Sumner, 2010). The consequences of this switch in flow regime are observed through the mean drag coefficient of the cylinders. For  $L^* < L_c^*$ , the mean coefficient of drag the downstream cylinder,  $C_{D_2}$ , is negative while it changes to a positive value for  $L^* > L_c^*$ . A similarly significant jump is also seen in the fluctuating drag and lift coefficients,  $\sigma_{C_D}$  and  $\sigma_{C_L}$ , of downstream cylinders at  $L_c^*$  (Alam *et al.*, 2003) (here,  $\sigma_x$  indicates the standard deviation of  $x$ ). Determination of this critical pitch ratio for the flow scenario more relevant to high Reynolds number engineered structures, i.e., rough cylinders in the postcritical regime, forms the first objective of this study.

In the reattachment regime at smaller pitch ratios, shear layers emanating from the upstream cylinder reattach alternately onto the downstream cylinder while steady reattachment is observed at intermediate distances (Igarashi, 1984; Alam *et al.*, 2003; and Sumner, 2010). Despite numerous studies, the exact nature of flow in the gap region in the reattachment regime is still uncertain. In the subcritical regime, the gap region is found to contain quasi-steady vortices, intermittent shedding, or an upstream jet near the centerline depending on  $L^*$  (Igarashi, 1984; Sumner, 2010). While more recent studies (Aasland *et al.*, 2023; 2022; Lin *et al.*, 2002) investigated the flow structure in detail using direct numerical analysis (DNS), stability analysis, or particle image velocimetry (PIV), these studies focused on only a few pitch ratios and low Reynolds numbers,  $Re \leq \mathcal{O}(10^4)$ . A comprehensive work investigating more pitch ratios is necessary to better understand the flow phenomena in the postcritical regime and the gradual changes induced with varying pitch. This forms the second objective of the current investigation.

Alam *et al.* (2003) found a local maximum in the fluctuating coefficients,  $\sigma_{C_{L,max}} = 0.8$  at  $L^* = 2.4$  that was linked to a minimum in the angle at which the shear layers from the upstream cylinder reattach on the downstream cylinder. It was later proposed that this minimum occurs due to the variation in the location of laminar to turbulent transition in the shear layers post separation from the upstream cylinder (Alam, 2014). The fluctuating forces ( $\sigma_{C_D}$  and  $\sigma_{C_L}$ ) on the downstream

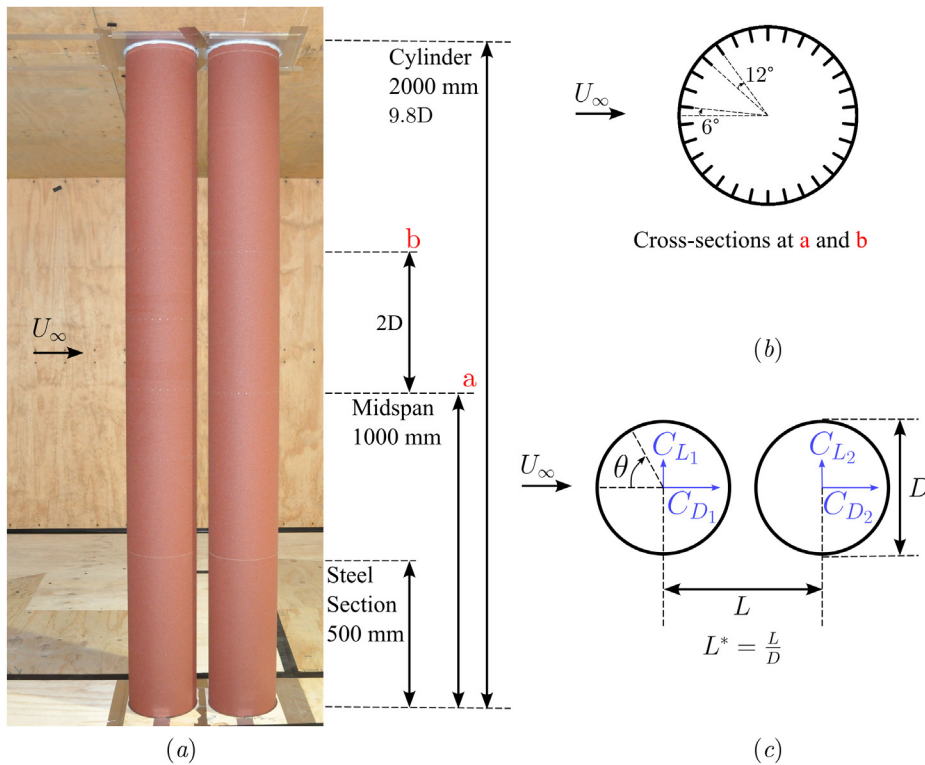


**FIG. 2.** Schematic of the setup. (a) Two cylinders installed in the wind tunnel at  $L^* = 1.175$ , (b) azimuthal distribution of pressure ports, and (c) definitions of various terms.

cylinder at  $L^* = 2.4$  reported in [Alam et al. \(2003\)](#) and [Alam \(2014\)](#) were as large as  $\sim 2.5$  times those seen on an isolated cylinder. In the current study, the incoming Reynolds number is in the postcritical regime. Since the boundary layer on the upstream cylinder would be turbulent before separation, this local maxima is expected to be absent. Given the limited knowledge of fluctuations in the lift and drag, the current investigation aims to confirm the absence of this maximum and provide estimates of the fluctuations in lift and drag in the postcritical scenario.

[Table I](#) further highlights the lack of a comprehensive study on rough, inline cylinders in postcritical flows. As mentioned previously, very few studies have so far dealt with postcritical flows. Exceptions are [Okajima \(1979\)](#) at  $6.2 \times 10^5$  with a rough upstream cylinder, [Gu et al. \(1993\)](#) at  $6.5 \times 10^5$  with turbulent inflow, and [Schewe and Jacobs \(2019\)](#) at  $10^7$  but only for three pitch ratios. Even fewer studies have considered rough cylinders ([Okajima, 1979](#); [Zdravkovich, 1980](#); and [Dubois and Andrianne, 2022](#)). [Okajima \(1979\)](#) applied surface

roughness only to the upstream cylinder to reduce the critical Reynolds number. [Zdravkovich \(1980\)](#) made use of sandpaper to simulate high Reynolds numbers on two *finite* and staggered cylinders. Recently, [Dubois and Andrianne \(2022\)](#) studied the influence of pitch ratio and Reynolds number on inline cylinders with a relative surface roughness ratio of  $k/D = 7.2 \times 10^{-3}$ . While they measured the unsteady forces on the cylinders, the maximum  $L^*$  tested was only 1.8, and hence the existence of a local peak (similar to [Alam et al., 2003](#)) in the fluctuating properties remains uncertain.

In addition, the majority of the investigations on inline cylinders have used cross-sectional pressure measurements to obtain the drag and lift coefficients for a given configuration ([Sumner, 2010](#); [Zhou and Alam, 2016](#)). A few ([Zdravkovich and Pridden, 1977](#); [Alam et al., 2003](#); and [Schewe et al., 2021](#)) have employed direct force measurements. Neither circumferential pressures at a single cross section nor force measurements provide information about the spanwise variation of the flow patterns. Thus, it is uncertain whether the transitions in

**TABLE I.** A non-exhaustive list of previous experimental investigations concerning inline cylinders in postcritical flows.

Investigation	Reynolds number(s)	Pitch ratios	Surface roughness
<a href="#">Okajima (1979)</a>	$0.4 - 6.5 \times 10^5$	1.07–6.3	Rough upstream cylinder
<a href="#">Gu et al. (1993)<sup>a</sup></a>	$6.5 \times 10^5$	1.05–7	Smooth cylinder
<a href="#">Schewe et al. (2021)</a>	$8 \times 10^5 - 10^7$	1.56, 2.8, 4	Smooth cylinder
<a href="#">Dubois and Andrianne (2022)</a>	$0.2 - 4 \times 10^5$	1.2–1.8	Two rough cylinders, $k/D = 7.2 \times 10^{-3}$
Current	$3 - 6 \times 10^5$	1.175–10	Two rough cylinders, $k/D = 1.28 \times 10^{-3}$ , $k_s/D = 1.9 \times 10^{-3}$

<sup>a</sup>Incoming turbulence,  $Tu = 10\%$ .

flow between various regimes occur over the entire span of the cylinder simultaneously. Carmo *et al.* (2010) reported cell structures across the span for a Reynolds number of 200 using stability analysis and numerical simulations. More recently, Aasland *et al.* (2022) observed cellular bi-stability for a Reynolds number of  $10^4$  using direct numerical simulations. However, experimental investigations of the spanwise structure appear absent, especially for postcritical flows. Knowledge of spanwise variations is critical in determining the overall loads in engineering applications.

To summarize, the current investigation is aimed at understanding the postcritical flow over inline cylinders with an emphasis on addressing the following uncertainties:

1. What is the critical pitch ratio in the postcritical flow regime? How does a further increase in Reynolds number impact the force coefficients?
2. How do the reattachment and wake flow patterns vary with pitch ratio in the reattachment regime?
3. Do the prominent maxima in the fluctuations of drag and lift seen in the subcritical regime exist in the postcritical regime? In their absence, how do the fluctuations vary with the pitch ratio?
4. How does the shear layer reattachment in the bistable regime and inside the reattachment regime vary across the span? Is there a variation with pitch ratio?

The remainder of this article is split into three sections. Sec. II describes the experimental setup used in this investigation and discusses the data acquisition and processing techniques. Section III presents the results and the corresponding analysis and discussion. Section IV concludes this work with a summary of the important perspectives and findings.

## II. METHODOLOGY

The experiments were conducted in a closed loop wind tunnel with a rectangular cross section of  $2000 \times 4000 \text{ mm}^2$ . The turbulence intensity of the incoming flow was measured to be 1.35%. The displacement and momentum thickness of both the roof and floor boundary layers at this position are  $\approx 12$  and  $\approx 10 \text{ mm}$ , respectively. The mean velocity at any point outside the boundary layers is within 0.5% of the global mean in the vertical center plane.

The two cylinders used are of equal diameter of  $D = 204 \text{ mm}$ . For all the tests except the largest pitch ratio, the downstream cylinder is at the streamwise center of the constant-area section while the upstream cylinder is translated on rails to adjust the pitch ratio,  $L^*$ . The downstream cylinder is installed vertically at 4600 mm from the start of the constant-area test section. Both the cylinders span the entire vertical dimension (2000 mm) of the working section, thereby resulting in an aspect ratio of  $\sim 9.8$  and a blockage ratio of 5.1%. The surface of the cylinder is made rough by wrapping it with P60 sandpaper (see Pasam *et al.*, 2023 for further details). The mean thickness of the sandpaper is included in the diameter, and the resulting relative roughness is  $k/D = 1.28 \times 10^{-3}$ , where  $k$  is the average sand-grain diameter on the sandpaper specified by the manufacturer. A conversion factor of  $k_s/k = 1.5$  is applied, which is obtained from the results of Achenbach and Heinecke (1981) and Speidel (1954), thereby giving  $k_s/D = 1.9 \times 10^{-3}$ . Here,  $k_s$  is the equivalent sand-grain roughness that results in a similar frictional velocity deficit in a fully rough channel flow (Nikurdase, 1933).

On each cylinder, two cross sections, one at the middle of the span and another two diameters above the mid-plane, are instrumented in order to measure the instantaneous surface pressure distributions. Each of these planes contain 30 pressure ports distributed uniformly in the azimuthal coordinate. The geometry of the setup is given in Fig. 2. Pressure from these ports was measured at 2000 Hz using a Turbulent Flow Instrumentation (TFI) Dynamic Pressure Measurement System. These measurements were taken for a minimum of 120 s, which encompasses  $\approx 2000$  shedding cycles. Longer samples ( $\approx 4000$  shedding cycles) were taken for pitch ratios where the flow is observed to be bistable in nature. A transfer function was applied to pressure measurements based on the diameter and length of the pressure tubing according to Bergh and Tijdeman (1965). The time-varying pressure signals were transformed into the frequency domain, and this transfer function was applied before transforming the data back into time domain. The cutoff frequency for pressure signals was chosen to be the frequency at which the theoretical amplitude response falls below 0.25, at  $f \approx 630 \text{ Hz}$ . The largest shedding frequency in the current tests is  $\approx 50 \text{ Hz}$  and the Kelvin-Helmholtz (K-H) frequencies reported in Sec. III F 3 are  $\approx 400 \text{ Hz}$ . Mean and fluctuating cross-sectional force coefficients are obtained by integrating the circumferential pressure distributions.

The aerodynamic force coefficients of each cylinder are represented using

$$C_{\chi_{\eta\alpha}} = \frac{F_{\chi_{\eta\alpha}}}{0.5\rho U_\infty^2 D}, \quad (1)$$

where  $\chi \in \{D, L\}$ ,  $\eta \in \{1, 2\}$ , and  $\alpha \in \{a, b\}$ . Here, 1 and 2 indicate the upstream and the downstream cylinders, respectively, while  $a$  and  $b$  indicate the locations of measurement at the midspan and two diameters above the span, respectively. Coefficients without the subscripts ( $a$  or  $b$ ) indicate the spanwise averages on the cylinder. The dimensional forces,  $F_D$  and  $F_L$ , are the (pressure) drag and lift, respectively, with  $C_D$  and  $C_L$  the corresponding drag and lift coefficients. Finally,  $\rho$  and  $U_\infty$  are the freestream density and velocity, respectively. Further details on the setup are provided in the study by Pasam *et al.* (2023), which documented the flow over a roughened single cylinder.

## III. RESULTS AND DISCUSSION

Figure 3 provides the variation of the sectional mean drag coefficient with the Reynolds number of the isolated roughened cylinders that were tested in the current setup. Note that all the data presented in Fig. 3 are corrected for the blockage following the procedure outlined in Roshko (1961) (originally proposed by Allen and Vincenti, 1944 and later verified by Farrell *et al.*, 1977). The results are in good agreement with previous works that incorporate similar relative roughnesses, thus validating the setup used. The variation of the isolated  $C_D$  between the two cylinders of the same roughness used in the current work is  $< 3\%$  over the range of Reynolds numbers presented and is  $\sim 1\%$  at  $Re = 3 \times 10^5$ . Note that the results from the two cylinder system were not modified to account for the wall interference since the influence of proximity of walls on the interactions between the two cylinders and the applicability of corrections is uncertain.

### A. Mean and fluctuating force coefficients

Figures 4(a) and 4(b) give the variation of the mean coefficient of drag,  $C_D$ , for each cylinder, with a pitch ratio,  $L^*$ , for a Reynolds

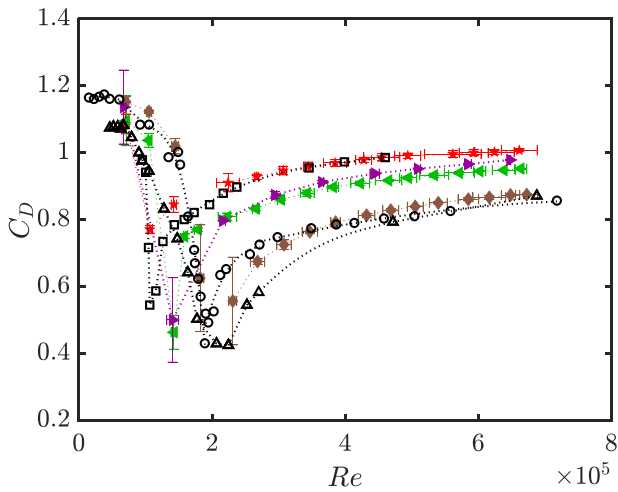


**FIG. 3.** Comparison of the blockage-corrected mean drag coefficient of the isolated cylinder with previous studies.  $\dots\dots\Delta\dots\dots$ : Achenbach (1971),  $k_s/D = 1.1 \times 10^{-3}$ ;  $\dots\dots\circ\dots\dots$ : van Hinsberg (2015),  $k_s/D = 1.2 \times 10^{-3}$ ;  $\dots\dots\square\dots\dots$ : Güven et al. (1980),  $k_s/D = 3.11 \times 10^{-3}$ ; dotted brown-filled diamond: Pasam et al. (2023),  $k_s/D = 1.1 \times 10^{-3}$ ; dotted red asterisk: Pasam et al. (2023),  $k_s/D = 3 \times 10^{-3}$ . Dotted left-pointed green-filled triangle: upstream cylinder in the current work,  $k_s/D = 1.9 \times 10^{-3}$ ; dotted right-pointed purple-filled triangle: downstream cylinder in the current work,  $k_s/D = 1.9 \times 10^{-3}$ .

number of  $3 \times 10^5$ . While Fig. 4(a) gives a comparison with a representative result for smooth inline cylinders in subcritical flow, Fig. 4(b) provides a comparison of the results from previous investigations of rough cylinders inline. Note that Okajima (1979) only roughened the upstream cylinder by covering it with thin polystyrene.

When the downstream cylinder is positioned far downstream at  $L^* = 10$ , the mean coefficient of drag of the upstream cylinder,  $C_{D_1}$ , is very close to that of a single isolated cylinder of the same roughness at

the same Reynolds number. As the downstream cylinder is moved closer, at pitch ratios of  $3.25 < L^* \leq 4$ ,  $C_{D_1}$  increases by a small amount due to the aerodynamic interference of the downstream cylinder.

As  $L^*$  is decreased further, the shear layers of the upstream cylinder reattach for the first time at  $L^* = 3.25$ , albeit only intermittently. The temporal prevalence of reattachment can be ascertained from the mean  $C_{D_1}$  of the upstream cylinder. Specifically,  $C_{D_1}$  when the shear layers reattach on the downstream cylinder is lower than that when they roll up in front of it and hence, lower  $C_{D_1}$  in the bistable region over the test duration (120 s or a non-dimensional time of  $2.4 \times 10^4$ , based on the convective timescale, i.e.,  $t^* = tU_\infty/D$ ) indicates a longer reattachment. Thus, from Fig. 4, it is evident that at  $L^* = 3.125$ , the shear layers reattach more often on the downstream cylinder and roll up occasionally. The pitch ratio range of  $3 < L^* \leq 3.25$  covers the bistable region for an incident Reynolds number of  $3 \times 10^5$ . This bistability and the intermittency are further explored in Sec. III E.

The smallest pitch ratio at which co-shedding is dominant, the critical pitch ratio,  $L_c^*$ , is found to be 3.25 in the current study. For subcritical flows, critical pitch ratios reported in the literature span the range 3–5 (Sumner, 2010) and tend to get smaller as the Reynolds number is increased. This is due to the concomitant decrease in formation length as Reynolds number increases. Ljungkrona et al. (1991) reported a positive correlation between the critical pitch ratio and the formation length as Reynolds number is changed.

For smooth inline cylinders at a much lower  $Re$  ( $\approx 2 \times 10^4$ ), Ljungkrona et al. (1991) found an  $L_c^*$  of 3.25 and 1.4 for incident flows with turbulence intensities of 0.1% and 1.4%, respectively. Incident turbulence intensity in the current investigation is 1.3%, but  $L_c^*$  is 3.25. However, Ljungkrona et al. (1991) investigated a much lower Reynolds number than considered here. An increased turbulence intensity in flow over smooth cylinders in the upper subcritical regime can cause early transition to the critical regime. Consequently, the formation length and thus the critical pitch ratio can change notably. An

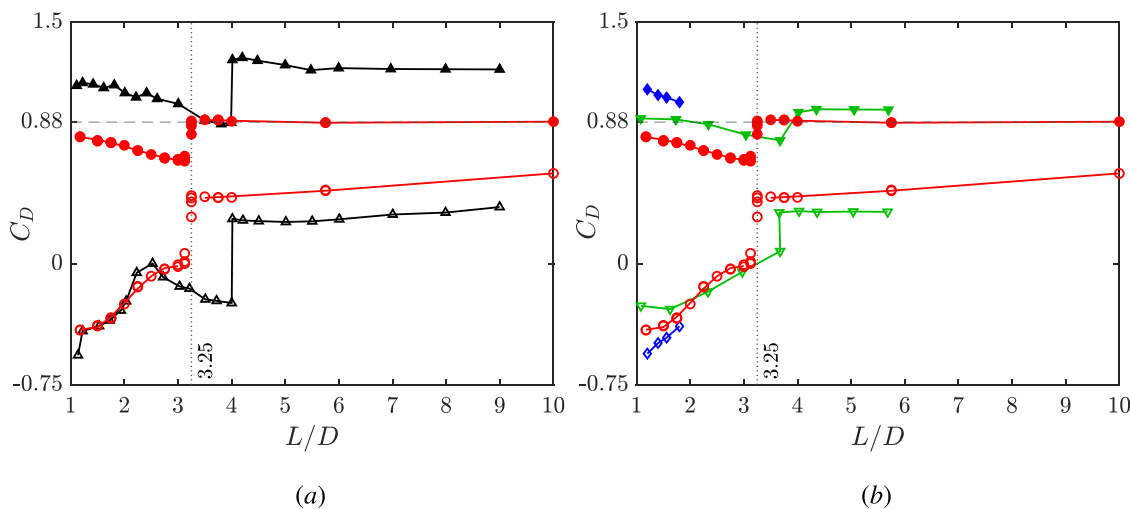


**FIG. 4.** A comparison of the variation of the mean drag coefficient with pitch ratio from different works [both (a) and (b)—split for clarity].  $\text{---}\Delta\text{---}$ : Alam et al. (2003); down-pointed green triangle: Okajima (1979); blue diamond: Dubois and Andrienne (2022); red circle: current,  $Re = 3 \times 10^5$ . Filled symbols: Upstream cylinder ( $C_{D_1}$ ). Empty symbols: downstream cylinder ( $C_{D_2}$ );  $\text{---}$ : isolated cylinder (see Table I for differences in setup across investigations).

increase in turbulence intensity in postcritical flows is expected to have a less prominent influence.

The mean drag coefficient of the downstream cylinder,  $C_{D_2}$ , at the largest pitch ratio tested ( $L^* = 10$ ) is only 60% of that of an isolated cylinder. This could be partly due to the use of a higher velocity for normalization that is incident on the downstream cylinder and is discussed in Sec. III D.  $C_{D_2}$  decreases as it is moved further upstream in the reattachment regime.  $C_{D_2}$  when the upstream shear layers are reattaching on the downstream cylinder is considerably lower than the  $C_{D_2}$  in the co-shedding regime and is negative (i.e., the downstream cylinder experiences thrust). During reattachment, the pressure over the forward surface of the downstream cylinder is lower than that on the rear surface, thus causing a suction toward upstream that results in negative drag. The pressure distribution on the downstream cylinder is further discussed in Sec. III E.

The agreement in the mean drag coefficient across different investigations is better for the downstream cylinder inside the reattachment regime than for the upstream cylinder or the downstream

cylinder outside the reattachment regime. Inside the reattachment regime ( $L^* < L_c^*$ ), the incoming flow and the ensuing boundary layer on the downstream cylinder are highly turbulent. Thus, the influence of the surface roughness or Reynolds number on the boundary-layer development and the resulting separation on the downstream cylinder is small. Recently, Aasland *et al.* (2022) noted the similarity in the separation angle of the downstream cylinder across investigations of different Reynolds numbers. It was conjectured that the flow phenomena in the reattachment regime could be described by a single parameter, i.e., the pitch ratio. This agreement seen in the mean drag coefficient of the downstream cylinder supports this conjecture. However, fluctuations in the drag and lift forces are dependent on the Reynolds number.

Figure 5 gives the variation of the fluctuating lift and drag coefficients of the two cylinders with a pitch ratio at  $Re = 3 \times 10^5$ . As the downstream cylinder is moved closer to the upstream cylinder, the fluctuations in the lift and drag of both cylinders increase up to a critical pitch ratio,  $L_c^*$ . Post shear layer reattachment on the downstream

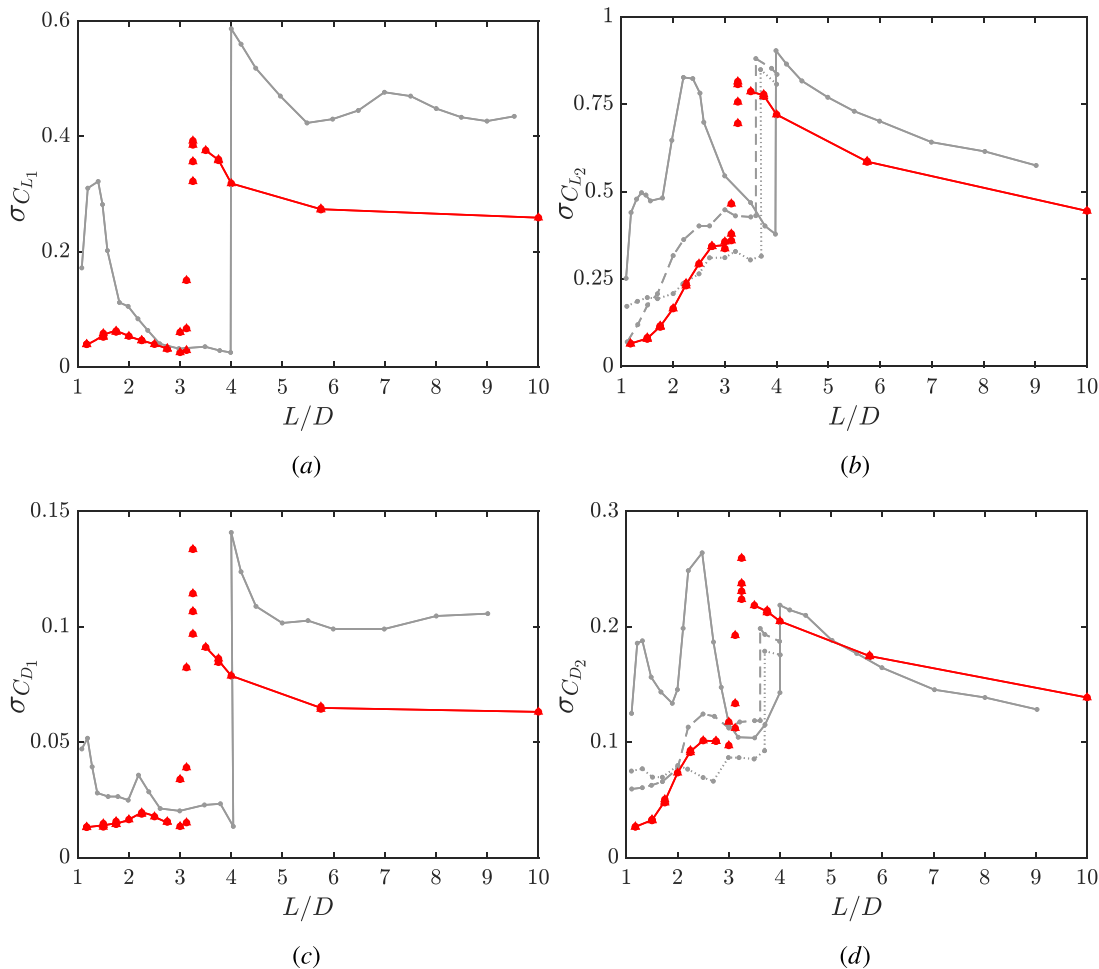
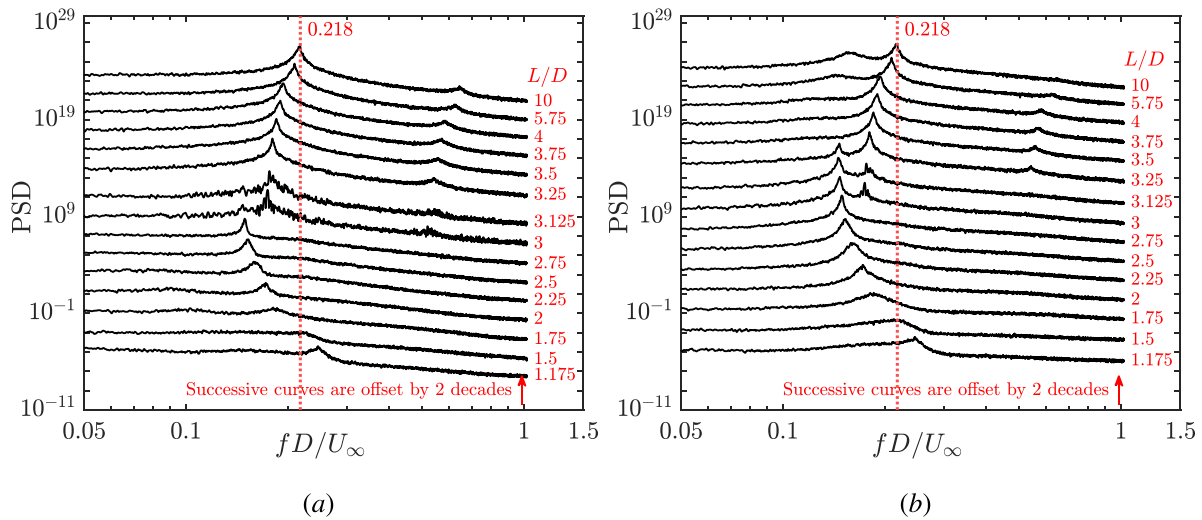


FIG. 5. The variation of fluctuating coefficients of forces with pitch ratio. —: Alam *et al.* (2003),  $Re = 6.5 \times 10^4$ , .....: Alam (2014),  $Re = 9.7 \times 10^3$ , ---: Alam (2014),  $Re = 1.6 \times 10^4$ , red-filled triangle: current,  $Re \approx 3 \times 10^5$ . (a) and (b) Fluctuating lift coefficient. (c) and (d) Fluctuating drag coefficient. (a) and (c) Upstream cylinder and (b) and (d) downstream cylinder.



**FIG. 6.** Power spectral density of the fluctuations in lift at different pitch ratios for  $Re \approx 3 \times 10^5$ . (a) Upstream cylinder and (b) downstream cylinder. Notice that the spectra from  $L^* = 1.5$  are offset by  $10^2$  from the previous  $L^*$  to increase clarity.

cylinder, these fluctuations decrease until they reach a minimum at the closest pitch ratio. Interestingly, Alam *et al.* (2003) and Alam (2014) reported local peaks in the fluctuating lift and drag for Reynolds numbers of  $Re = 6.5 \times 10^4$  and  $3.2 \times 10^4$ , but not for  $Re = 9.7 \times 10^3$  and  $1.6 \times 10^4$ . These maxima in the fluctuating drag and lift increased in magnitude as Reynolds number was increased and reached values as high as 2.8 and 2 times of that for an isolated cylinder, respectively. A peak of such prominence is absent in the current study at  $Re = 3 \times 10^5$ . This is discussed further in Sec. III G 2.

## B. Frequency spectra of lift fluctuations and Strouhal number

Figure 6 shows the power spectral density of the lift fluctuations of the two cylinders at different pitch ratios and an incoming Reynolds number of  $3 \times 10^5$ . Each spectrum reported is obtained from the time history of lift coefficient fluctuations recorded for  $\approx 6000$  shedding cycles. Each spectrum is also the average of the spectra obtained from the two measurement locations (one at midspan and the other two diameters above the span) and those obtained from the repeat tests for a given pitch ratio.

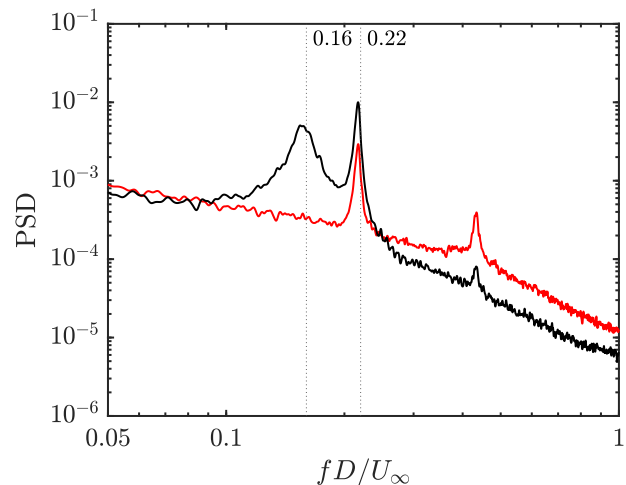
At large pitch ratios ( $L^* = 10$ ), a dominant frequency is seen in the spectra of both cylinders, which is similar to that of an isolated cylinder at the same Reynolds number ( $St = fD/U_\infty \approx 0.22$  for isolated cylinder of the same roughness at  $Re \approx 3 \times 10^5$ ). The lift fluctuations of the upstream cylinder also contain a prominent third harmonic, indicating that the flow is closer to the isolated scenario. On the other hand, the spectrum of the downstream cylinder contains an additional less prominent peak near  $St \approx 0.16$ .

Figure 7 gives the power spectral density of the pressure fluctuations on the downstream cylinder at a pitch ratio of  $L^* = 10$  and an incoming Reynolds number of  $3 \times 10^5$ . Note that these spectra are also averages of those measured at the two cross sections. While the spectra of pressure near the stagnation ( $\theta = 6^\circ$ ) show a prominent peak at  $fD/U_\infty \approx 0.22$  and its second harmonic, the spectra near the

separation point ( $\theta = 90^\circ$ ) have another frequency, at  $fD/U_\infty \approx 0.16$ . Given that  $fD/U_\infty \approx 0.22$  is the shedding frequency of the upstream cylinder, the second, lower frequency  $fD/U_\infty \approx 0.16$  corresponds to the asynchronous shedding from the downstream cylinder. This second frequency appears in the lift spectrum of the downstream cylinder even at  $L^* = 5.75$ .

As the pitch ratio is reduced, synchronization of the shedding between the two cylinders increases. This is evident from the existence of only one prominent shedding frequency (and its third harmonic) in the lift spectra of the downstream cylinder for  $L^* \leq 4$ .

Thus, for the parameter space investigated, the co-shedding regime can be further classified into two regions,  $3.25 < L^* \leq 4$ , where the shedding between the two cylinders is synchronous, and



**FIG. 7.** Power spectral density of the fluctuations in the surface pressure of the downstream cylinder at  $L^* = 10$  and  $Re \approx 3 \times 10^5$ . Red line:  $\theta = 6^\circ$ , —:  $\theta = 90^\circ$ .



$L^* \geq 5.75$ , where the downstream cylinder sheds at a different frequency. Shown in Fig. 8, Okajima and Sugitani (1984) found two frequencies behind the downstream cylinder for  $L^* \geq 6$ , while Alam and Zhou (2008) found two frequencies at  $L^* = 5$ .

Within the bistable region, two prominent peaks are seen in the lift spectra of the downstream cylinder corresponding to the two flow regimes, i.e., reattachment and co-shedding. The peak at the higher frequency is due to the co-shedding configuration, while the smaller frequency peak is due to the reattachment configuration. At  $L^* = 3.25$ , the energy in the higher frequency peak is more than that of the lower frequency peak, indicating a longer prevalence of the co-shedding regime. As the pitch ratio is decreased, reattachment of the shear layers occurs for a longer duration and the corresponding lower frequency peak contains higher energy. At  $L^* = 3$ , the higher frequency peak is less prominent, and at  $L^* = 2.75$ , it is absent in the spectra. This further substantiates that the bistable region for  $Re \approx 3 \times 10^5$  is  $3 < L^* \leq 3.25$ . On the other hand, the lift spectra of the upstream cylinder in the bistable region are more scattered despite containing a peak at the frequency corresponding to the co-shedding flow.

In the reattachment regime, the lift spectra of the downstream cylinder contain a prominent frequency at all pitch ratios and the Strouhal number of the shedding increases with decreasing pitch ratio. The lift spectra of the upstream cylinder at pitch ratios of  $2 \leq L^* \leq 2.75$ , also contain the same prominent frequency. On the other hand, the spectra of the upstream cylinder at pitch ratios  $L^* = 1.5$  and  $1.75$  exhibit a broadband plateau. This indicates that the oscillations in the lift are less periodic. At the same pitch ratios, the spectra from downstream cylinder contain a dominant frequency but with a much lower prominence when compared to the peaks seen for  $2 \leq L^* \leq 2.75$ , hinting at a less organized shedding for these pitch ratios. At the closest pitch ratio tested,  $L^* = 1.175$ , a prominent

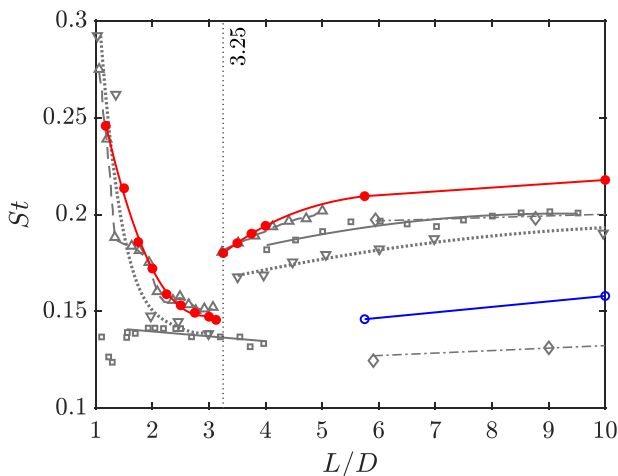


**FIG. 8.** Strouhal number of the lift fluctuations from the two cylinders at various pitch ratios. Red filled circle: Current, frequencies found on both the upstream and downstream cylinder,  $Re \approx 3 \times 10^5$ ; blue circle: current, frequencies found on only the downstream cylinder,  $Re \approx 3 \times 10^5$ ; for smooth, inline cylinders -  $\square$  - Alam et al. (2003),  $Re = 6.5 \times 10^4$ ;  $\triangle$  - Igarashi (1981),  $Re = 3.5 \times 10^4$ ;  $\nabla$  - Xu and Zhou (2004),  $Re = 4.2 \times 10^4$ ;  $\diamond$  - Okajima and Sugitani (1984),  $Re = 1.6 \times 10^4$ .

shedding frequency reappears in the lift spectrum of the upstream cylinder, marking a return of strong periodicity. Flow configurations and the nature of shedding within the reattachment regime are addressed in further detail in Sec. III F.

The Strouhal numbers of shedding from the downstream cylinder for different pitch ratios are given in Fig. 8. As the pitch ratio is decreased from  $L^* = 10$ , the Strouhal number decreases. A decrease in Strouhal number along with an increasing  $C_{D1}$  indicates that the wake width of the upstream cylinder increases as the downstream cylinder moves upstream. This is due to the deceleration of the wake flow near the centerline caused by the downstream cylinder.

As seen from the spectra, a lower Strouhal number is observed when the flow pattern changes from predominantly co-shedding to predominantly reattachment. Within the reattachment regime, the Strouhal number increases as  $L^*$  decreases. The highest Strouhal number is observed at the closest pitch ratio tested, and this value is larger than that of an isolated cylinder at the same Reynolds number. The trends in Strouhal number vs pitch ratio are similar to those found on smooth cylinders in the study by Igarashi (1981) and Xu and Zhou (2004). The magnitude of the Strouhal numbers in the current investigation is in excellent agreement with those reported in the study by Igarashi (1984) despite the large difference in Reynolds numbers. Within the reattachment regime, Alam et al. (2003) and Alam (2014) reported a nearly constant Strouhal number, in contrast to the results from the other investigations including the current one.

### C. Summary of flow behavior at different pitch ratios

Table II gives a brief overview of the flow behavior across the pitch ratios investigated. The *co-shedding regime* exists for  $L^* > 3.25$ , and it has been further subdivided based on whether vortex shedding from the cylinders is synchronized. The key features of this regime are discussed in Sec. III D. Moving to smaller pitch ratios, shear layers separating from the upstream cylinder reattach intermittently onto the downstream cylinder in the *bistable regime* that spans  $3 < L^* \leq 3.25$ . Flow behavior in the bistable regime is analyzed in Sec. III E.

At closer spacings still, *stable asymmetric gap flow* is found within the range  $1.5 \leq L^* < 2.25$ . This asymmetry arises from the partial reattachment of the shear layer emanating from one side of the upstream cylinder. The flow structure at these pitch ratios is characterized by two anti-symmetric modes that transition between each other intermittently. These modes are not distinguishable in the range  $2.25 < L^* \leq 3$ . The reattachment pitch ratio range is thus demarcated into the “alternating reattachment regime” for  $1.5 \leq L^* < 2.25$  and the “continuous reattachment regime” for  $2.25 < L^* \leq 3$ . Finally, the gap flow becomes symmetric at the closest pitch ratio tested of  $L^* = 1.175$ . The reattachment regime covering  $L^* \leq 3$  is described in detail in Sec. III F.

The Reynolds number of the incoming flow is maintained at  $\approx 3 \times 10^5$  for the results presented in these sections. Section III G describes the influence of Reynolds number on various flow parameters for  $3 \times 10^5 \leq Re \leq 6 \times 10^5$ . Finally, Sec. IV summarizes the results.

### D. Co-shedding regime $L^* > 3.25$

The co-shedding regime exists at pitch ratios beyond the critical pitch ratio, i.e.,  $L^* > L_c^*$ , characterized by vortex shedding from both the upstream and downstream cylinders.

TABLE II. Summary of the flow configurations observed at different pitch ratios.



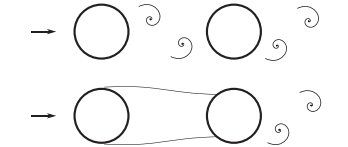
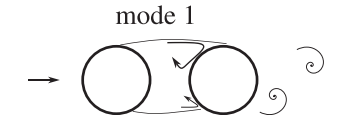


Pitch ratio	Flow configuration	Characteristics
$L^* \geq 5.75$		<b>Co-shedding regime</b> Both the cylinders shed vortices. The downstream cylinder sheds at a different frequency.
$3.25 < L^* \leq 4$		Both the cylinders shed vortices at the same frequency.
$3 < L^* \leq 3.25$		<b>Bistable regime</b> Shear layers from the upstream cylinder reattach on the downstream cylinder occasionally. They reattach more often as $L^*$ or $Re$ decreases. Reattachment occurs over spanwise extent of at least two diameters.
(a) $2.25 < L^* \leq 3$	(a) and (b) 	(a) Continuous reattachment regime: The two modes are nearly indistinguishable. Transitions between the two modes occur at a high frequency. Fluctuations in the lift of the upstream cylinder contain prominent frequency.
(b) $1.5 \leq L^* < 2.25$		(b) Alternating reattachment regime: Two modes are distinct. Transitions occur only sporadically. Modes also alternate across sections of span. Fluctuations in the lift of the upstream cylinder are weakly periodic.
$L^* = 1.175$		Gap flow is symmetric with prominent vortices in both the halves. A prominent frequency reappears in the lift spectra of the upstream cylinder.

Figure 9 gives the distribution of the mean and the fluctuating pressure coefficients on the circumference of the two cylinders at pitch ratios beyond the critical pitch ratio along with that for an isolated cylinder at a Reynolds number of  $Re \approx 3 \times 10^5$ . Coefficients reported for each cylinder are the average of measurements at the two spanwise cross sections.

Similar to the force coefficients, the circumferential pressure distributions on the upstream cylinder are closer to those of an isolated cylinder at the largest pitch ratio tested ( $L^* = 10$ ). On the upstream cylinder, the mean pressures near the separation angle, i.e.,  $90^\circ \leq \theta \leq 140^\circ$ , and upstream of it, i.e.,  $54^\circ \leq \theta \leq 90^\circ$ , are slightly larger than the isolated cylinder and increase with decreasing pitch ratio.

On the downstream cylinder, the mean pressure near the stagnation point,  $0^\circ \leq \theta \leq 35^\circ$ , decreases as the pitch ratio is decreased.

Minimum pressure increases as the pitch ratio decreases, and the location of minimum pressure moves slightly downstream. Near the base region,  $100^\circ \leq \theta \leq 180^\circ$  [Fig. 9(d)], the mean pressure increases as the pitch ratio is increased from  $L^* = 3.5$  to  $L^* = 5.75$  but decreases from  $L^* = 5.75$  to  $L^* = 10$ . A similar trend was seen in the study by Zdravkovich (1977), where base pressure increased up to  $L^* = 5$  but decreased with a further increase from  $L^* = 5$  to  $L^* = 7$ , thus resulting in a local maximum in the base pressure at  $L^* = 5$ .

As discussed in Sec. III B, frequency spectra reveal that the downstream cylinder exhibits a distinct periodic vortex shedding for  $L^* \geq 5.75$  at a frequency different from that of the upstream cylinder. This suggests that the flow over the downstream cylinder may be similar to a highly turbulent flow impinging on an isolated cylinder for  $L^* \geq 5.75$ , albeit with the significant frequency of impinging vortices

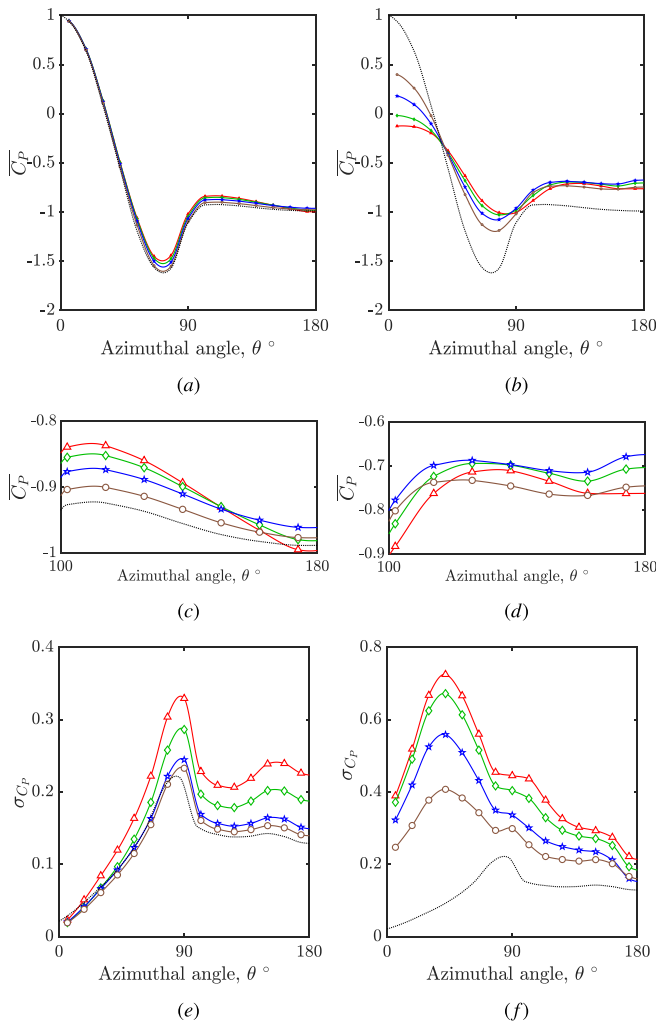


**FIG. 9.** Pressure coefficients in the co-shedding regime in  $Re \approx 3 \times 10^5$ . (a), (c), and (e) Circumferential pressure coefficients on the upstream cylinder. (b), (d), and (f) Circumferential pressure coefficients on the downstream cylinder. (a)–(d) Mean pressures. (e) and (f) Fluctuating pressures. ....: Isolated cylinder, brown circle:  $L^* = 10$ , blue asterisk:  $L^* = 5.75$ , green diamond:  $L^* = 4$ , and red triangle:  $L^* = 3.5$ .

present. Indeed, beyond the critical pitch ratio, the incident flow onto the downstream cylinder will have high unsteadiness and will also have a lower effective Reynolds number at  $L^* = 5.75$  than at  $L^* = 10$  due to a lower oncoming mean velocity from the wake of the upstream cylinder.

An increase in Reynolds number causes an increase in the minimum pressure coefficient and a decrease in the base pressure coefficient for an isolated cylinder for a fixed incoming turbulence intensity (Pasam et al., 2023). A decrease in the turbulence intensity causes an increase in both minimum pressure and base pressure coefficients (Cheung 1983) for a fixed Reynolds number. Thus, if the flow over the downstream cylinder is similar to that of an isolated cylinder, the minimum pressure coefficient at  $L^* = 10$  is expected to be higher than that

at  $L^* = 5.75$ . This is in contradiction to the minimum pressure being lower at  $L^* = 10$  than at  $L^* = 5.75$  seen in Fig. 9(b).

A potential reason behind this apparent discrepancy is the use of the free-stream velocity and reference static pressure for normalizing the pressure distributions. The effective incoming flow velocity for the downstream cylinder is different from the upstream cylinder and depends on the pitch ratio. In addition, the downstream cylinder experiences cross-stream pressure and velocity gradients from being in the wake of the upstream cylinder. It sees both a lower dynamic pressure and a lower total pressure. A common normalization based on the free-stream velocity and pressure can thus introduce additional uncertainty while comparing pressure distributions across large changes in pitch ratio. This explains the discrepancy in the variation of pressure distributions between  $L^* = 5.75$  and  $L^* = 10$  compared to what would be expected for a simple change in  $Re$  and turbulence intensity on an isolated cylinder.

This (partially) explains why the apparent drag coefficient of the downstream cylinder is only 60% of that seen for an isolated cylinder, even at pitch ratios as large as  $L^* = 10$ . For instance, the Strouhal number measured on the downstream cylinder is  $\approx 0.16$  based on  $U_\infty$  as the reference velocity. The Strouhal number of shedding behind a rough cylinder is  $\sim 0.2$ , except in the critical regime. This suggests that the “effective flow velocity” seen by the downstream cylinder at  $L^* = 10$  could be  $\approx U_\infty/1.25$ . If we use this scaled velocity as the reference velocity, the “true drag coefficient” of the downstream cylinder would appear to be  $\approx 93\%$  of that seen for an isolated cylinder.

Within the co-shedding regime, the mean re-circulation region in the wake of the upstream cylinder widens in the cross-stream direction and shortens in the streamwise direction as the downstream cylinder is moved closer. As  $L^*$  is reduced from  $\sim 4$ , the drag coefficient of the upstream cylinder increases and the Strouhal number decreases, indicating a wake widening. Further, the pressure fluctuations in the base region of the upstream cylinder increase, indicating a closer vortex roll up.

The fluctuations in the pressure distribution on the downstream cylinder are much larger than those observed on an isolated cylinder at the same Reynolds number, and increase as the pitch ratio is decreased. These distributions contain three local maxima. The most upstream peak at  $\theta \approx 42^\circ$  corresponds to the fluctuations caused by impinging vortices shed from the upstream cylinder. A less prominent plateau near  $90^\circ \leq \theta \leq 102^\circ$  corresponds to boundary-layer separation on the cylinder, while an even smaller plateau at  $152^\circ \leq \theta \leq 164^\circ$  corresponds to the shear layer roll up post separation. As the pitch ratio decreases, the position of the second peak moves further downstream along with a reduction in prominence, indicating a less distinct but more downstream separation as the downstream cylinder is moved toward the upstream cylinder.

### E. Bistable regime, $3 < L^* \leq 3.25$

This regime corresponds to the region where the separated shear layers from the upstream cylinder intermittently reattach onto the surface of the downstream cylinder. Schematics of the two stable modes observed in this regime are given in Fig. 10. These flow configurations can be identified in time histories of the coefficients of drag and lift of the two cylinders (plotted against dimensionless convective time,

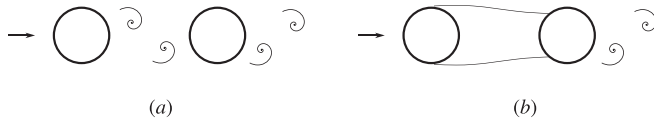


**FIG. 10.** Schematics of the two flow configurations in the bistable regime. (a) Co-shedding mode and (b) reattachment mode.

$t^* = tU_\infty/D$ ) seen in Fig. 11. The coefficients are recorded for  $L^* = 3.125$  and for a Reynolds number of  $Re \approx 3 \times 10^5$ .

The transition between the two configurations is effectively instantaneous across the span of two diameters. In addition, small bursts ( $\approx 100$  convective cycles, or  $\approx 20$  shedding cycles) of the co-shedding regime were observed at  $+2D$ , but not at midspan (for instance, at  $t^* \approx 1 \times 10^4$ ).

The co-shedding configuration can be identified by a higher mean  $C_D$  on both cylinders along with higher fluctuations in both  $C_D$  and  $C_L$ . The two modes, co-shedding and reattachment, are separated using two filters where (a) a moving median of  $C_D$  over 100 convective cycles is more than four standard deviations away from the nominal mean  $C_D$  (of the moving median) observed in the reattachment regime and (b) fluctuations in the  $C_L$  are more than four standard deviations away from the nominal  $\sigma_{C_L}$  observed in the reattachment regime. The nominal values are obtained from the reattachment regime observed at the same pitch ratio and Reynolds number.

Based on this mode separation, the mean and fluctuating pressure distributions observed at  $L^* = 3.125$  and  $Re \approx 3 \times 10^5$  are given in Fig. 12. The mean and the fluctuating pressure distributions on both cylinders in the co-shedding configuration resemble those seen at higher pitch ratios (shown in Fig. 9).

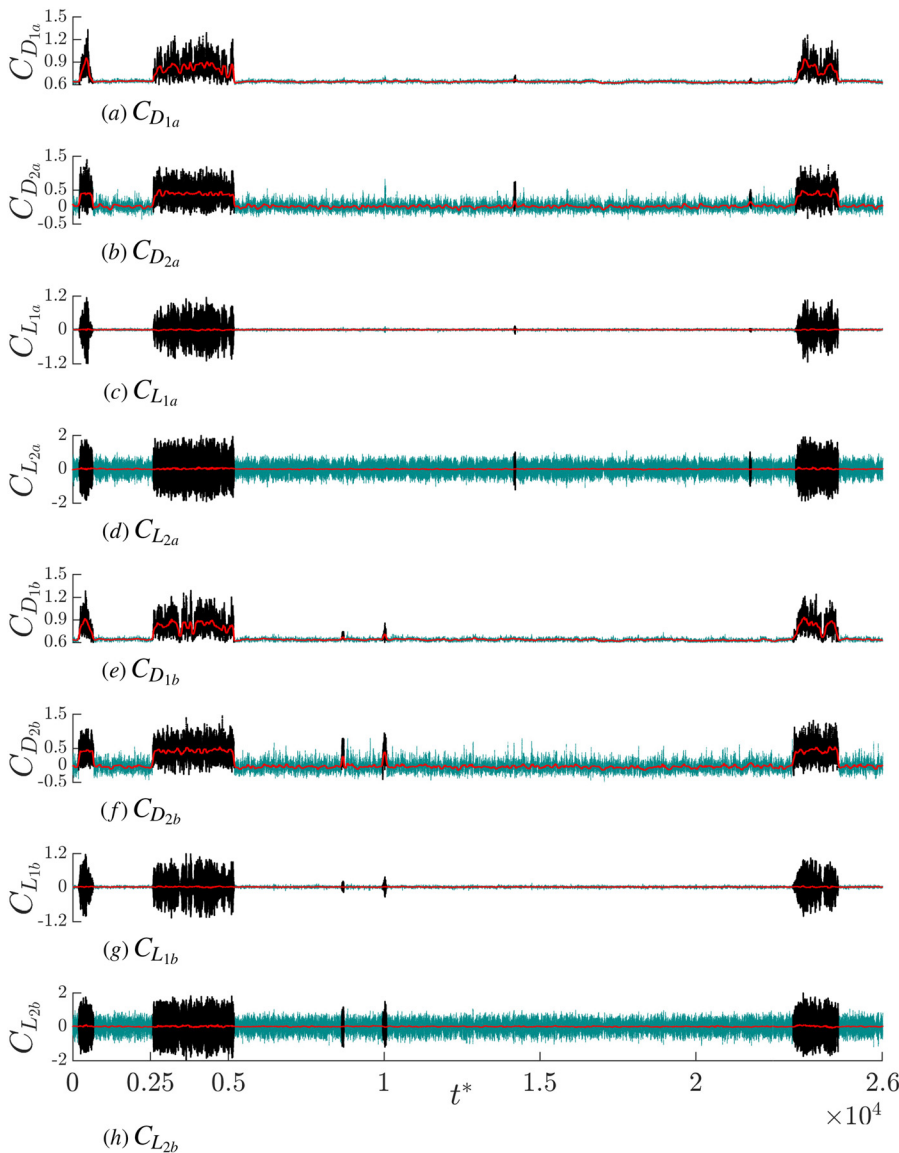


**FIG. 11.** Time histories of the force coefficients of the two cylinders at the two measurement planes for a pitch ratio of  $L^* = 3.125$  and  $Re \approx 3 \times 10^5$ . —: co-shedding mode, cyan line: reattachment mode. Red line: Moving median of 100 convective time cycles. [See Eq. (1) for subscript notation.]

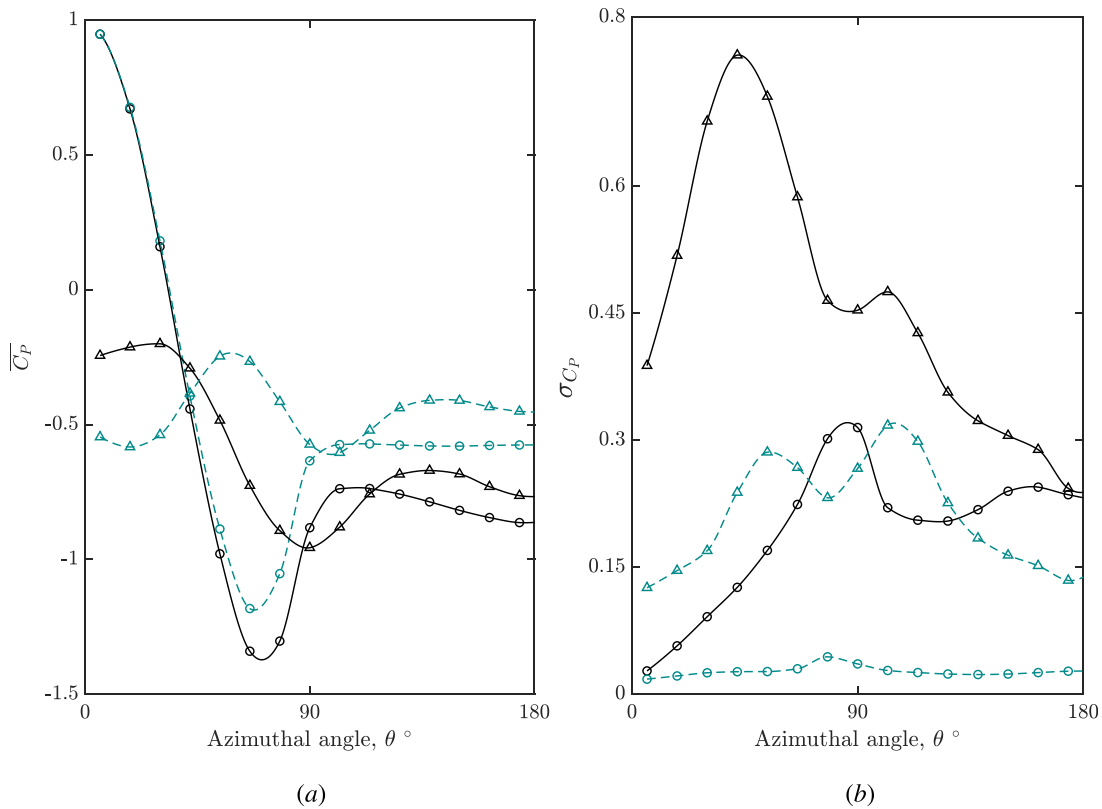


**FIG. 12.** (a) Mean and (b) fluctuating circumferential pressure distributions at a pitch ratio of  $L^* = 3.125$  and  $Re \approx 3 \times 10^5$ . —: Co-shedding, cyan dashed line: reattachment.  $\Delta$ : Downstream cylinder,  $\circ$ : upstream cylinder.

When the upstream shear layers reattach onto the downstream cylinder, the fluctuations in the region enclosed by the two cylinders and the two upstream shear layers are relatively lower than those observed behind an isolated cylinder. This results in a flatter mean pressure distribution on the upstream cylinder over  $100^\circ \leq \theta \leq 180^\circ$ . In addition, the pressure over the upstream surface ( $0^\circ \leq \theta \leq 30^\circ$ ) of the downstream cylinder is of the same magnitude as that near the downstream surface ( $100^\circ \leq \theta \leq 180^\circ$ ) of the upstream cylinder. On the downstream cylinder, the global maximum of the mean pressure distribution is seen at  $\approx 60^\circ$ , and this corresponds to the reattachment of the upstream shear layers.

On the upstream cylinder, the minimum pressure just upstream of the separation region increases in the reattachment regime from that observed in the co-shedding regime. While this increase acts to locally increase  $C_{D_i}$ , the increase in the base pressure due to reattachment acts to decrease  $C_{D_i}$  by a larger amount, thereby resulting in an overall decrease in  $C_{D_i}$  when the shear layers reattach.

Fluctuating pressure distributions on both the upstream and downstream cylinders reduce by a significant amount when the separated shear layers from the upstream cylinder re-attach onto the downstream cylinder. When the shear layers reattach, two peaks are observed in the fluctuating pressure distribution of the downstream cylinder. The upstream peak corresponds to the position where the separated shear layers from the upstream cylinder reattach onto the downstream cylinder. The second peak corresponds to the separation

of the boundary layers on the downstream cylinder. The location of the second peak is further downstream but within  $\approx 12^\circ$  of that observed in the co-shedding configuration. This indicates that the location of separation moves downstream when the shear layers reattach onto the downstream cylinder.

Figure 13 gives the intermittency factor,  $\gamma$ , defined as the ratio of the duration of the co-shedding mode to the total test duration for  $3 \leq L^* \leq 3.5$ . It is clear that the co-shedding mode exists for the entirety of the test duration at  $L^* = 3.5$ . At  $L^* = 3.25$ , shear layers reattach intermittently and co-shedding is predominant ( $\gamma > 0.5$ ). Shear-layer reattachment is dominant at  $L^* = 3.125$ . At  $L^* = 3$ , there is negligible presence of the co-shedding mode. These observations confirm the existence of the bistable flow for  $3 < L^* \leq 3.25$ .

### F. Reattachment regime, $1.175 \leq L^* \leq 3$

This section explains the flow behavior in the reattachment regime that spans  $1.175 \leq L^* \leq 3$  in the current study. Two modes of reattachment found previously in subcritical flow over smooth tandem cylinders are introduced first. The behavior of the shear layers in these modes and the consequent aerodynamic forces on the two cylinders in postcritical flow are then explained in detail. The discussion then focuses on the variation of the two modes with the pitch ratio and the behavior of the flow at the two measurement locations across the span of each cylinder.

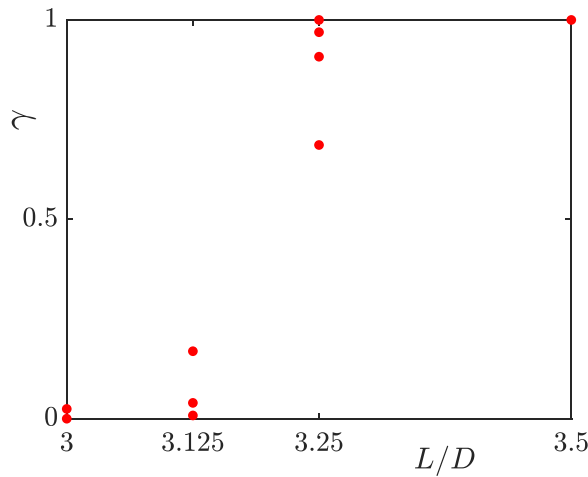


FIG. 13. Variation of intermittency factor with pitch ratio at  $Re \approx 3 \times 10^5$ .

1. The two reattachment modes

Within the reattachment regime, intermittent asymmetric flow configurations were previously observed in the study by Lin et al. (2002), Zhou et al. (2019), and Aasland et al. (2023) at low Reynolds numbers ( $Re \leq 10^3$ ). In these flow configurations, the shear layer emanating from one half of the upstream cylinder partially overshoots the downstream cylinder while that from the other half reattaches entirely. A schematic of these flow configurations is given in Fig. 14. These modes are also found in the current investigation where  $Re > 3 \times 10^5$ .

Figure 15 gives the variation of the lift coefficient on the four measurement planes over time for a pitch ratio of  $L^* = 1.75$  for  $Re \approx 3 \times 10^5$ , where the intermittent modes are observed. For a fixed spanwise position, fluctuations about a mean positive cross-sectional lift coefficient are seen on the upstream cylinder while the downstream cylinder experiences a mean negative lift at the same spanwise cross

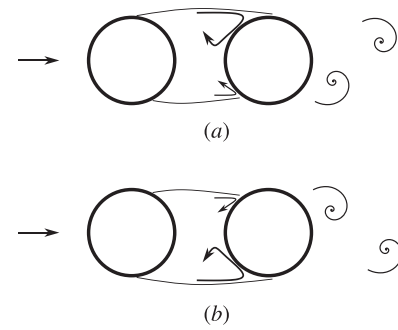


FIG. 14. (a) and (b) The two flow configurations within the reattachment regime.

section. After a period, the cross-sectional lift coefficients switch signs, i.e., the upstream cylinder experiences a mean negative cross-sectional lift while the downstream cylinder experiences a mean positive lift. For clarity, the flow configuration leading to a negative lift coefficient on the upstream cylinder,  $C_{L1}$ , is referred to as mode 1, while a positive  $C_{L1}$  is considered mode 2.

The mean flow configuration over the duration of test ( $> 2.5 \times 10^4$  convective cycles) is biased, i.e., one of the modes occurs more often than the other. This asymmetry is indicative of the high sensitivity of the reattaching shear layers to minor asymmetries, if any, in the setup. Lin et al. (2002), with the help of PIV in the gap between the two cylinders, also found asymmetric averaged flow structures at  $L^* = 1.5$ . Asymmetry in the pressure distribution and gap vortices at similar pitch ratios has also been reported in other investigations (Aasland et al., 2023; Zhang and Melbourne, 1992; and Ljungkrona et al., 1991).

In order to analyze the two modes further, a moving median filter of 100 convective cycles is applied and the modes are then separated based on the sign of the filtered lift coefficient. The mean and fluctuating pressure distributions on the two cylinders for the test data of Fig. 15 are given in Fig. 16. These distributions are obtained after

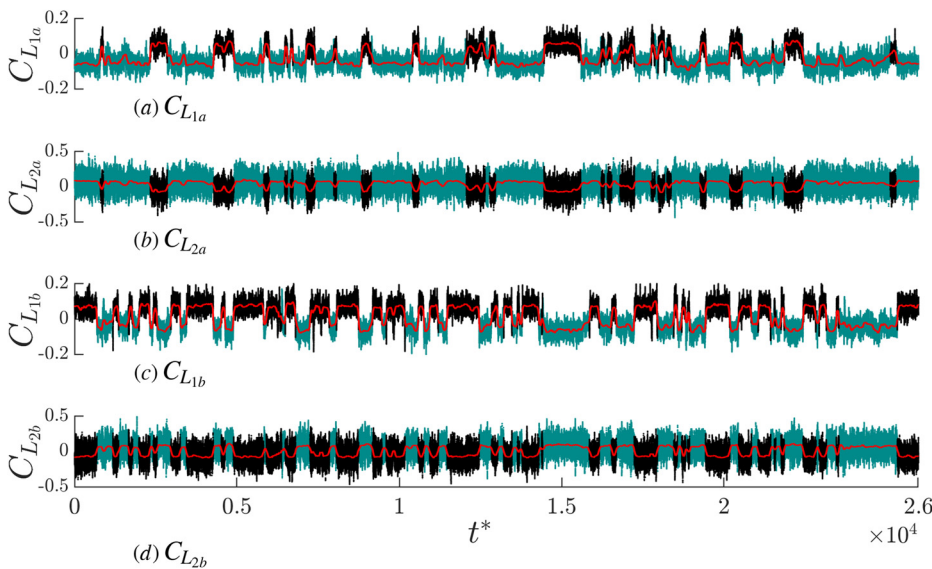
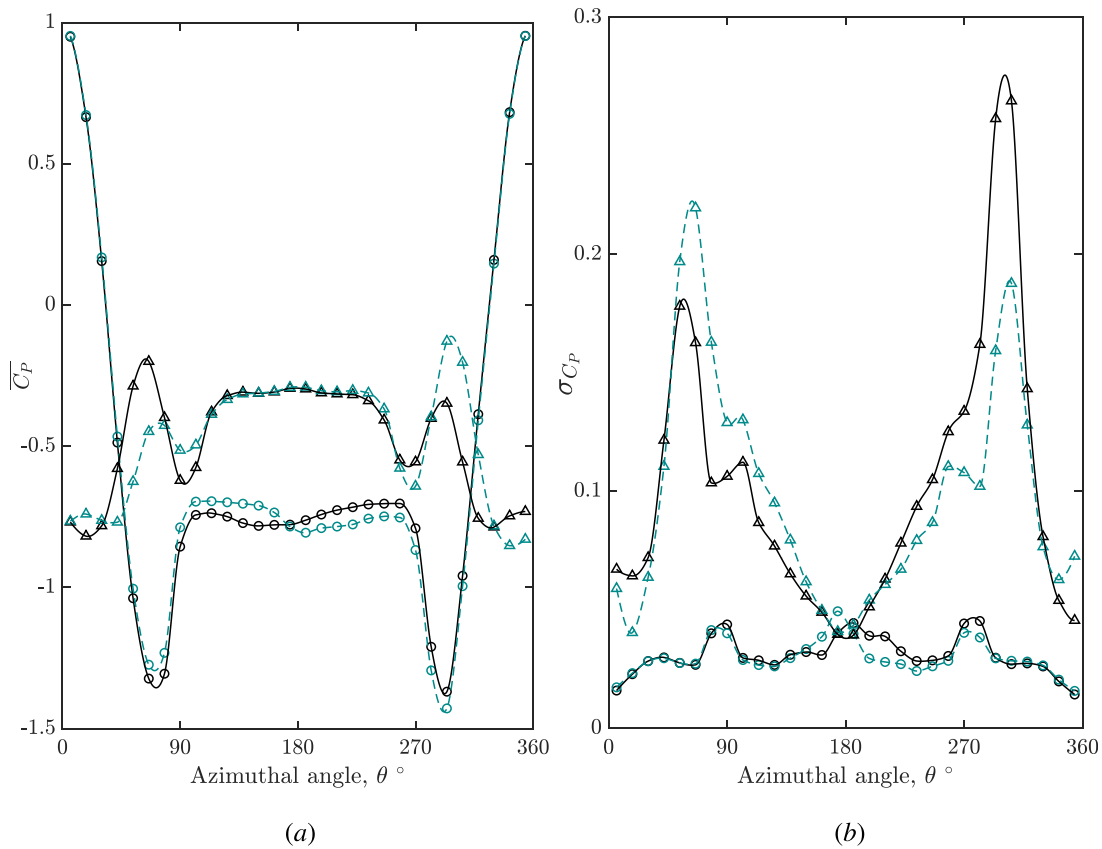


FIG. 15. Time history of the lift coefficients of the two cylinders at the two measurement planes for a pitch ratio of  $L^* = 1.75$  and  $Re \approx 3 \times 10^5$ . Cyan line: Mode 1, —: mode 2. Red line: Moving median of 100 convective cycles. [See Eq. (1) for subscript notation.]



**FIG. 16.** (a) Mean and (b) fluctuating surface pressure distributions at a pitch ratio of  $L^* = 1.75$  and  $Re \approx 3 \times 10^5$ . Cyan dashed line: Negative lift coefficient on the upstream cylinder (mode 1), —: positive lift coefficient on the upstream cylinder (mode 2).  $\Delta$ : Downstream cylinder,  $\circ$ : Upstream cylinder.

averaging the “mode separated” measurements at the two spanwise cross sections.

Consider the mean pressure distributions on each cylinder in the range  $0^\circ \leq \theta \leq 180^\circ$ . On the upstream cylinder, mode 1 corresponds to a larger base pressure than mode 2. In addition, the minimum pressure is larger for mode 1, indicating larger deceleration of the flow than that seen in mode 2. Previous work by [Güven et al. \(1980\)](#) and [Pasam et al. \(2023\)](#) indicates that the angle of intersection of the “straight line fit of the pressure distribution in the region of pressure rise ( $90^\circ \leq \theta \leq 100^\circ$ ) and the base pressure” is a useful estimate of the separation angle. Based on this measure, the boundary layer on the upstream cylinder in mode 1 separates earlier than that in mode 2 for  $0^\circ \leq \theta \leq 180^\circ$ .

This earlier separation on one half of the cylinder results in a lift force pointing opposite to that half, since the pressure post separation is higher. Thus, mode 1 on the upstream cylinder results in a negative lift coefficient, i.e., with  $C_{L1}$  pointing toward  $180^\circ \leq \theta \leq 360^\circ$ . In the same half ( $0^\circ \leq \theta \leq 180^\circ$ ), the mean pressure distribution on the downstream cylinder indicates that reattachment occurs later in mode 1 than in mode 2. Moreover, the pressure rise due to reattachment is lower for mode 1 than for mode 2. This low pressure due to a later reattachment in one half of the cylinder causes a lift force pointing toward that half. Thus, mode 1 on the downstream cylinder results in a positive lift coefficient, i.e., with  $C_{L2}$  pointing toward  $0^\circ \leq \theta \leq 180^\circ$ .

If we now consider the fluctuating pressures, both mode 1 and mode 2 on the upstream cylinder result in a similar fluctuating pressure coefficient distribution, except over  $150^\circ \leq \theta \leq 180^\circ$ . Fluctuating pressure coefficients on the upstream cylinder corresponding to mode 1 over  $150^\circ \leq \theta \leq 180^\circ$  are larger than those in mode 2. For the downstream cylinder, the fluctuating pressure coefficients during mode 1 are larger than those during mode 2 over  $54^\circ \leq \theta \leq 180^\circ$ . The distributions for both modes still exhibit two peaks. As mentioned previously, the upstream peak is due to the reattachment of the separated shear layers and the downstream peak corresponds to the separating boundary layer on the downstream cylinder. In mode 1, the peak due to the separation on the downstream cylinder in  $0^\circ \leq \theta \leq 180^\circ$  is less prominent, indicating that the reattached shear layer interferes with the separation on the downstream cylinder.

In summary, an earlier separation of shear layers on one half of the upstream cylinder accompanies a later mean reattachment on the corresponding half of the downstream cylinder. This earlier separation on the upstream cylinder causes a lift force in the direction of the other half due to larger pressure near the separation region. On the other hand, later reattachment on the downstream cylinder causes a lift in the direction of the same half due to the lower pressure in the reattachment region. The later reattachment on the downstream cylinder also causes larger fluctuations near the reattachment region and less

distinct separation on the downstream cylinder. A schematic of the proposed mean flow for the two modes is given in Fig. 17.

Earlier separation on one half of the upstream cylinder and the later reattachment on the downstream cylinder is also evident in the PIV results of Lin *et al.* (2002). The half that experiences an earlier separation (i.e.,  $0^\circ \leq \theta \leq 180^\circ$  in mode 1) contains a region of strong vortices in the gap between the cylinders as seen in the study by Lin *et al.* (2002) and Aasland *et al.* (2023). This correlates well with the larger fluctuating pressures near the reattachment region over  $54^\circ \leq \theta \leq 180^\circ$  on the downstream cylinder and also in  $150^\circ \leq \theta \leq 180^\circ$  of the upstream cylinder seen for mode 1. Of course, mode 2 is simply a reflection of mode 1 about the line of symmetry (line joining the centers of the two cylinders). While these modes were identified previously, the current investigation gives a comparison of the mean separation and reattachment angles along with the consequent lift forces.

**2. Variation of the two modes with pitch ratio**

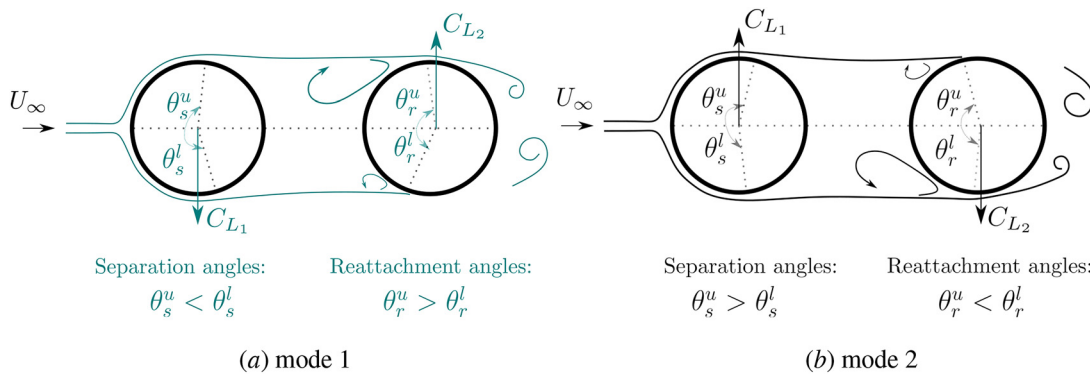
Figure 18 gives the time history of the lift coefficient on the upstream cylinder at midspan at different pitch ratios in the reattachment regime for  $Re \approx 3 \times 10^5$ . As the pitch ratio increases from  $L^* = 1.5$ , the difference in the sectional lift generated between the two modes decreases. The two modes are nearly indistinguishable for  $L^* > 2.25$  and  $L^* = 1.175$ . With increasing pitch ratio from  $L^* = 1.5$ , the frequency of switching between the modes also increases. An increase in switching frequency along with a decrease in difference between the modes results in a more symmetric mean flow configuration as the pitch ratio increases. Similar phenomena were found on smooth inline cylinders previously. Lin *et al.* (2002) observed the flow to be more symmetric at  $L^* = 2$  than at  $L^* = 1.5$ . Alam *et al.* (2003) reported that the shear layers reattach alternately for pitch ratios of  $1 < L^* < 3$  and steadily for  $3 < L^* < 4$ . In the current investigation, alternating reattachment is observed for  $1.5 \leq L^* < 2.25$ . The differences in the pitch ratios at which alternating and steady reattachment are observed are likely due to varying incoming flow conditions across investigations. Shear-layer behavior post separation from the upstream cylinder is expected to be sensitive to the incoming Reynolds number, turbulence intensity, and surface roughness of the cylinder.

Figure 19 gives the pressure distributions on the two cylinders at various pitch ratios within the reattachment regime. The plots are split into two halves, the left half represents the cylinder in mode 1 while the right half represents mode 2.

On the downstream cylinder, the nature of reattachment of the separated shear layer and the boundary-layer separation can be identified through the fluctuating pressure distributions given in Fig. 19(d). Consider a separated shear layer of a finite thickness. At a large pitch ratio within the reattachment regime (say  $L^* = 2.5$ ), all of the shear layer reattach onto the downstream cylinder. This reattachment results in a peak in the mean pressure distribution of the downstream cylinder. In addition, the reattachment occurs sufficiently upstream (i.e., smaller  $\theta$ ) such that a distinct boundary-layer separation exists on the downstream cylinder. As observed previously, this results in two distinct peaks in the fluctuating pressure distribution on the downstream cylinder. The upstream peak corresponds to the reattachment on the downstream cylinder while the downstream peak corresponds to the separation of the boundary layer.

As the pitch ratio is reduced, the outer part of the shear layer in mode 1 (left half) overshoots the downstream cylinder and interferes with the boundary-layer separation while the inner part reattaches onto the downstream cylinder (Zhou and Yiu, 2006; Aasland *et al.*, 2023). Thus, at closer pitch ratios and on the half with the later reattachment (and shear layer overshoot), fluctuating pressure distribution on the downstream cylinder would contain a less prominent peak corresponding to the separation of the boundary layer. At  $L^* = 1.5$ , there is only one prominent peak in the fluctuating pressure distribution on the downstream cylinder in mode 1 (left half), and it corresponds to the reattachment of the separated shear layers on the cylinder. At  $L^* = 1.5$ , the shedding frequency is less distinct for both the upstream and downstream cylinders, indicating a less organized shedding (see Fig. 6).

In addition, current results also indicate a correlation between the alternating reattachment and the relative magnitudes of fluctuations in pressure caused by reattachment and separation on the downstream cylinder. As the pitch ratio is decreased from  $L_c^*$ , alternating reattachment is first observed at  $L^* = 2.25$ . This is also the pitch ratio at which the pressure fluctuations on the downstream cylinder near the shear layer reattachment reach a similar magnitude to those due to the separation on the downstream cylinder. For  $L^* < 2.25$ , the fluctuations in



**FIG. 17.** Schematic of the time averaged flow in the two modes in the alternating reattachment regime,  $1.5 \leq L^* \leq 2$ . Subscripts s: separation, r: reattachment. Superscripts: u: upper half ( $0^\circ \leq \theta \leq 180^\circ$ ) and l: lower half ( $180^\circ \leq \theta \leq 360^\circ$ ).



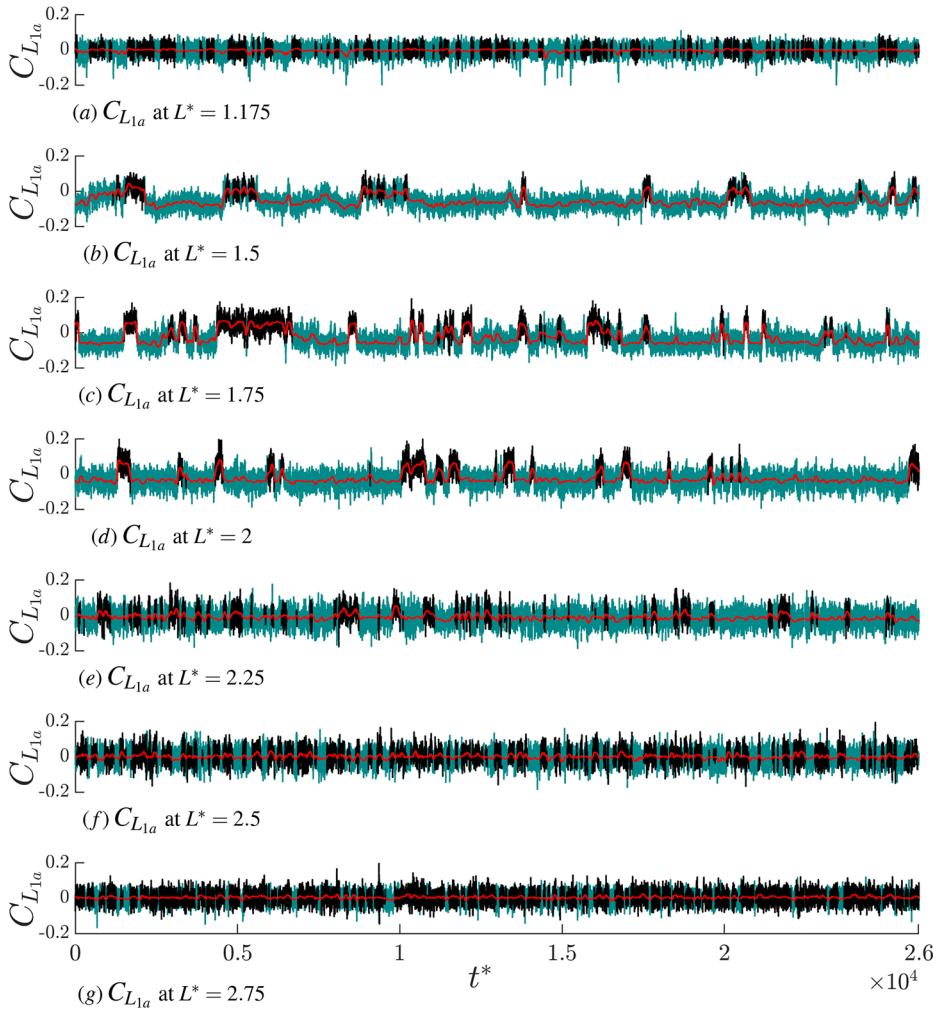


**FIG. 18.** Time history of the lift coefficients of the upstream cylinder at the midspan for  $Re \approx 3 \times 10^5$  and different pitch ratios. —: Mode 2, cyan line: mode 1. Red line: Moving median of 100 convective time cycles.

pressure on the downstream cylinder are larger near reattachment than near separation (for mode 1 shown in the left half of Fig. 19(d)).

The variation of mean  $C_D$  of either cylinder with the pitch ratio is a result of a few key changes in the mean pressure distribution. These changes are given as follows:

1. On the upstream cylinder [Fig. 19(a)] and for both the modes, the mean pressure near the separation region,  $54^\circ \leq \theta \leq 90^\circ$ , and the base of the upstream cylinder,  $90^\circ \leq \theta \leq 180^\circ$ , increase as the pitch ratio is increased. The decrease in  $C_{D_1}$  due to the increase in the base pressure is larger than the increase in  $C_{D_1}$  due to the increase in minimum pressure. Thus, the overall drag coefficient of the upstream cylinder decreases with an increase in pitch ratio.
2. On the downstream cylinder and for both the modes, the mean pressure in the upstream region ( $0^\circ \leq \theta \leq 42^\circ$ ) of the downstream cylinder increases with an increase in pitch ratio. The base pressure of the downstream cylinder decreases with an increase in pitch ratio in the range  $1.5 \leq L^* \leq 2.75$ . This results in an increase in the  $C_{D_2}$  as the pitch ratio is increased.

3. On the downstream cylinder for mode 1 [i.e., left half of Fig. 19(c)], the peak in the mean pressure due to reattachment is lower than the base pressure of the cylinder. As the pitch ratio is increased, this peak increases in magnitude and moves upstream.

The pressure distributions for the closest pitch ratio considered,  $L^* = 1.175$ , stand out in the trends of the fluctuating pressures on the upstream cylinder and both the mean and fluctuating pressures on the downstream cylinder. Moreover, a more prominent frequency in the lift fluctuation spectrum of the upstream cylinder is also found at this pitch ratio (see Fig. 6) unlike at  $L^* = 1.5$ . This indicates that the flow pattern at  $L^* = 1.175$  is different from the alternating reattachment observed at  $L^* = 1.5$ .

For  $L^* = 1.175$ , fluctuations near the base of the upstream cylinder are of similar magnitude to the fluctuations near the separation peak, indicating that a significant vortex roll up occurs near the base region at this pitch ratio. The mean and fluctuating pressure distributions on the downstream cylinder are similar for both the modes, indicating that the flow pattern is symmetric. Carmo *et al.* (2010) also found that flow is symmetric in the gap for  $L^* = 1.5$  and alternating

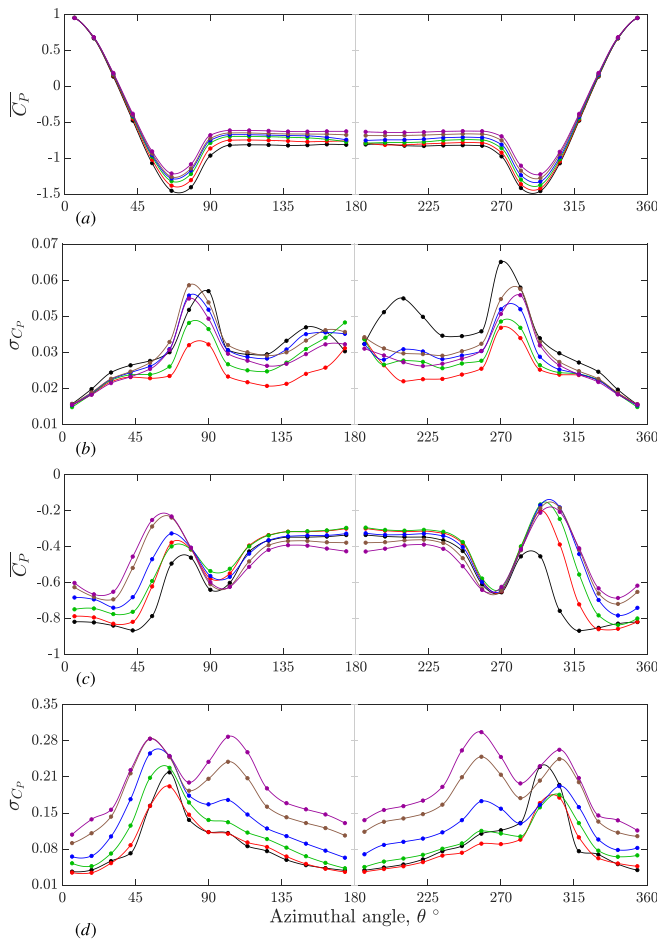


**FIG. 19.** Mode-averaged, circumferential pressure distributions on the two cylinders at various pitch ratios at  $Re \approx 3 \times 10^5$ . (a) and (c) Mean pressure coefficients, (b) and (d) fluctuating pressure coefficients, (a) and (b) upstream cylinder, and (c) and (d) downstream cylinder. Left: Mode 1, right: mode 2 (flipped).  $L^* =$  —: 1.175, red line: 1.5, green line: 1.75, blue line: 2, brown line: 2.25, purple line: 2.5.

in the gap for a larger pitch ratio ( $L^* = 1.8$ ) using DNS for  $Re = 200$ . Time averaged flow pattern in the gap at  $L^* = 1.175$  in the current investigation is given in Fig. 20.

### 3. Spectra of pressure fluctuations on the downstream cylinder

Figure 21 gives the frequency spectra of fluctuations in the pressure coefficient on the downstream cylinder for different pitch ratios in mode 1. The four locations on the surface shown correspond to

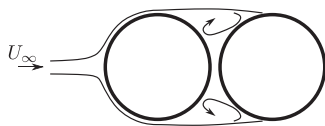


**FIG. 20.** Schematic representation of the time averaged gap flow at  $L^* = 1.175$ .

$\theta = \{54^\circ, 306^\circ, 90^\circ, 270^\circ\}$ . The two upstream angles  $\{54^\circ, 306^\circ\}$  are close to the upstream peak in  $\sigma_{C_p}$  on the downstream cylinder [see Fig. 19(d)]. Pressure measurements at these angles are hence expected to be more sensitive to the fluctuations in the separating shear layers from the upstream cylinder. On the other hand, the two downstream angles  $\{90^\circ, 270^\circ\}$  are close to the separation points on the downstream cylinder. Also provided are the spectra of pressure fluctuations at the corresponding locations for an isolated cylinder of the same roughness and facing the same Reynolds number.

Of interest is the additional frequency band (other than the shedding frequency) with larger energy than the neighborhood, for instance, at  $fD/U_\infty \approx 1 - 2$  in the spectra corresponding to  $L^* = 1.175, 1.5, 1.75$ . These frequencies are absent in the pressure spectra of an isolated cylinder. However, a similar frequency band related to the Kelvin–Helmholtz (K–H) instability was observed in the velocity fluctuations in the shear layer of an isolated cylinder at  $0.5D$  downstream that had disappeared by  $1D$  downstream (see Fig. 17 in Pasam et al., 2023). Kelvin–Helmholtz (K–H) shear layer fluctuations from the upstream cylinder in the current investigation are prominent in the pressure spectra until  $1.75D$  downstream. This suggests that the development of K–H fluctuations is suppressed in the presence of a downstream cylinder. Thus, it appears that the presence of the downstream cylinder has a stabilizing effect on the shear layers emanating from the upstream cylinder. Aasland et al. (2022) also reported a delayed onset of the K–H instability at  $L^* = 3$  for smooth cylinders at  $Re = 10^4$ .

Another feature of the spectra is that in mode 1 (for  $L^* = \{1.5, 1.75, 2\}$ ), the distribution of energy in the above-mentioned frequencies is sharper and at a slightly lower frequency for  $\theta = \{54^\circ, 90^\circ\}$  than for  $\theta = \{306^\circ, 270^\circ\}$ . This indicates that a vortex region of a slightly larger length scale and larger vorticity is found in the half corresponding to  $0^\circ \leq \theta \leq 180^\circ$  than in  $180^\circ \leq \theta \leq 360^\circ$  during mode 1, providing additional support for the existence of flow configurations proposed in Fig. 17.

To summarize, the mean flow configuration is asymmetric/biased for  $1.5 \leq L^* < 2.25$  while it is symmetric for  $2.25 < L^* \leq 3$ . Shear layers from the upstream cylinder reattach alternately for  $1.5 \leq L^* < 2.25$  and continuously for  $2.25 < L^* \leq 3$ . A signature of K–H fluctuations is observed in the spectra of the fluctuating pressure measurements on the surface of the downstream cylinder at the former pitch ratios, while this is absent for the latter. It is further evident that this broadband energy distribution decreases in prominence as  $L^*$  increases while the energy in the second harmonic increases. The second harmonic in shedding is prominent for  $L^* = 2.25$ . This indicates that the reattachment mode transitions from alternating to continuous when broadband fluctuations in the shear layer coalesce into a second harmonic of shedding frequency.

### 4. Spanwise flow structure

Evident from Fig. 15 is that the two modes alternate in the spanwise planes. When the flow configuration is mode 1 in the mid-plane, the cross-sectional plane at  $+2D$  experiences mode 2. This switch in the flow configurations can also be observed through correlation between the instantaneous coefficients of lift from the two planes at different pitch ratios. The coefficient of correlation ( $R_{C_L}$ ) between  $C_L$  measured at the two planes for various pitch ratios is given in Fig. 22.

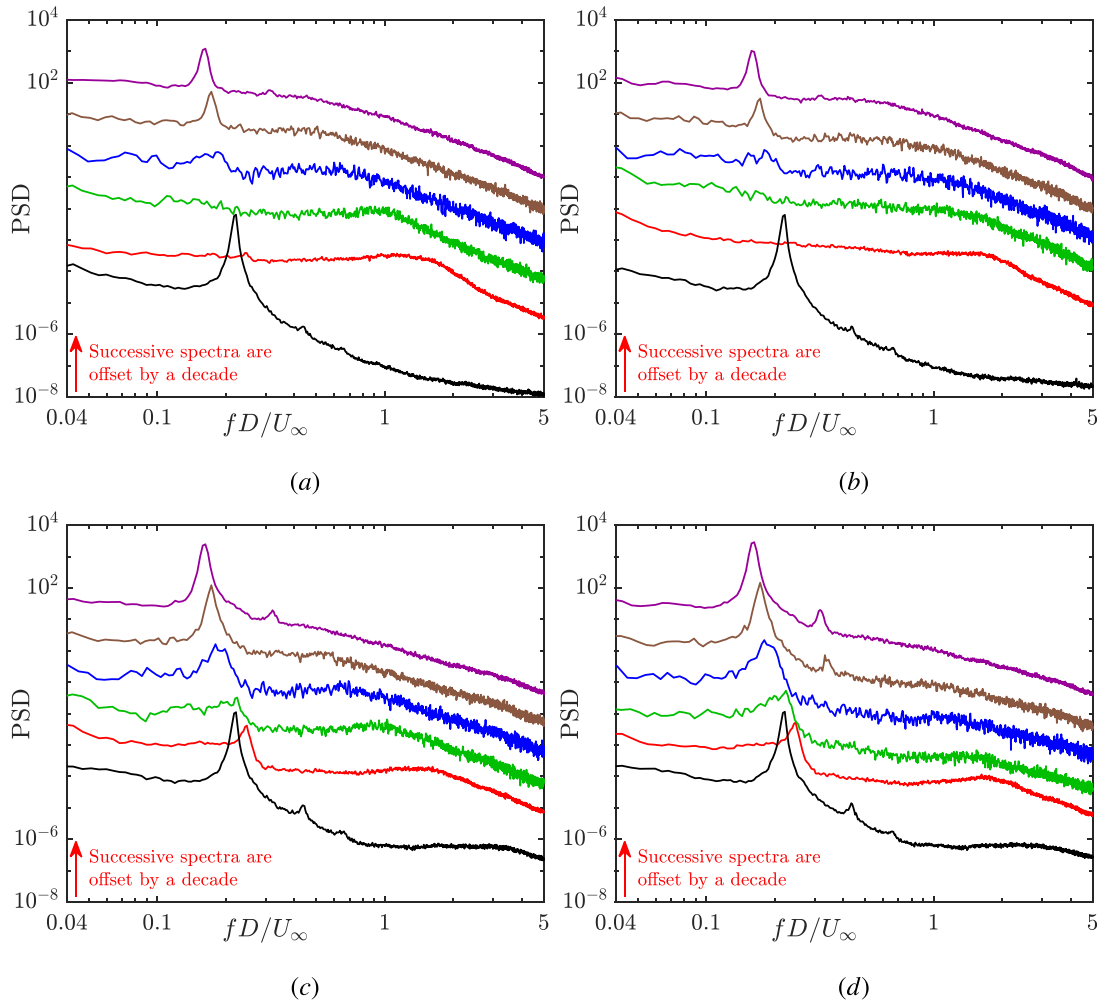


**FIG. 21.** Frequency spectra of surface pressure fluctuations on the downstream cylinder.  $Re \approx 6 \times 10^5$  (a)  $\theta = 54^\circ$ , (b)  $\theta = 306^\circ$ , (c)  $\theta = 90^\circ$ , and (d)  $\theta = 270^\circ$ . —:  $L^* = \infty$  (isolated cylinder), red line:  $L^* = 1.175$ , green line:  $L^* = 1.5$  in mode 1, blue line:  $L^* = 1.75$  in mode 1, brown line:  $L^* = 2$  in mode 1, and purple line:  $L^* = 2.25$ .

Figure 22 also contains the corresponding correlation measured on an isolated cylinder of the same roughness for comparison.

Spanwise correlation of lift for the upstream cylinder for all reattachment pitch ratios is lower than that for an isolated cylinder. As pitch ratio is reduced from  $L^* = 2.75$ , this correlation coefficient decreases, reaching a minimum for  $L^* \approx 1.5$  and then increases until  $L^* = 1.175$ . In addition, the correlation coefficient is negative for  $1.5 \leq L^* \leq 2$ , indicating that the instantaneous lift coefficients are often out of phase between the two spanwise planes. On the downstream cylinder, the spanwise correlation coefficient of the raw data at  $2.25 \leq L^* \leq 2.75$  is slightly larger than that seen for an isolated cylinder. It is positive for all pitch ratios in the reattachment regime, indicating that the instantaneous coefficients of lift are more often in the same direction.

To analyze the spanwise existence of modes, a moving median filter is applied with a window of 100 convective time cycles to the time history of the lift. The correlation between the median-filtered lift coefficients is also shown in Fig. 22. The corresponding filtered correlation

is  $\approx 0.1$  for an isolated cylinder. This relatively low correlation on the isolated cylinder is due to a lack of fluctuations of the scale of the filter width. In the inline configuration, the correlation between the filtered lift coefficients indicates that, in the case of alternating reattachment, spanwise planes at 0 and  $+2D$  experience opposite modes at a given instant of time. This implies that the cross section at midspan and at  $2D$  above midspan experiences median lift in the opposite direction. This is in good agreement with the alternating vorticity contours across span observed at a very low Reynolds number,  $Re = 415$  (through direct numerical simulations) in the study by Carmo *et al.* (2010) at  $L^* = 1.8$ .

To further investigate the spanwise distribution of the alternating flow structure, the upstream and downstream cylinders were interchanged and measurements of  $C_L$  on the downstream cylinder were performed at four different spanwise locations for a Reynolds number of  $3 \times 10^5$  and a pitch ratio of  $L^* = 1.75$ . The downstream cylinder in the original setup at  $L^* = 1.75$  and  $Re \approx 3 \times 10^5$  has  $C_D \approx -0.34$  and  $\sigma_{C_L} \approx 0.12$ . The downstream cylinder in the interchanged setup

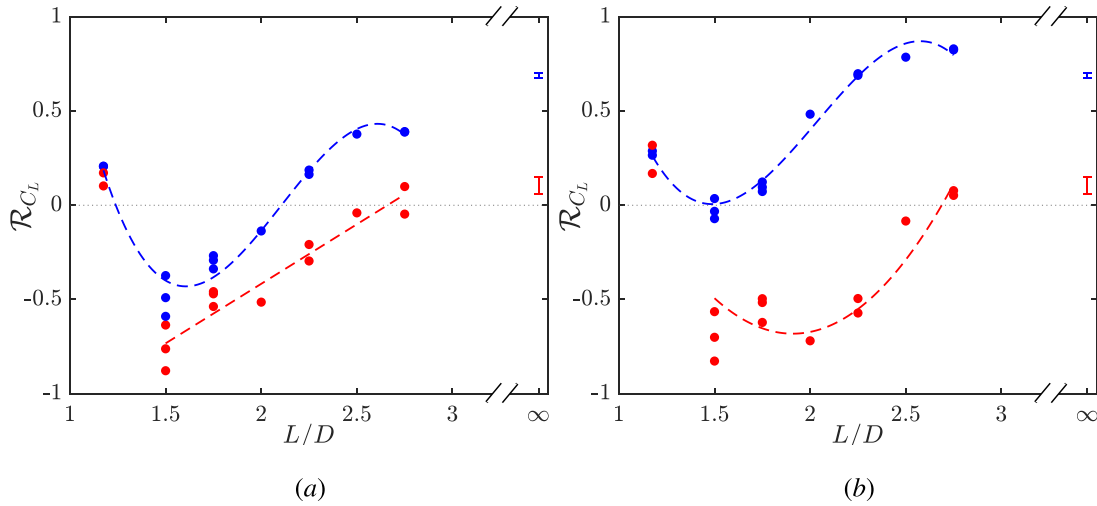


**FIG. 22.** Coefficient of correlation between the lift coefficients measured at the two spanwise positions, 0 and  $+2D$  at  $Re \approx 3 \times 10^5$ . (a) Upstream cylinder and (b) downstream cylinder. Blue dashed line: Correlation between instantaneous  $C_L$ , and red dotted-dashed line: correlation between the median filtered  $C_L$ . Error bars for the isolated cylinder correspond to 90% confidence intervals.

has  $\overline{C_D} \approx -0.35$  and  $\sigma_{C_L} \approx 0.11$ , indicating that there is no significant difference between the two setups.

The time histories of the lift coefficients at different spanwise locations on the downstream cylinder are shown in Fig. 23. The spanwise cross sections at  $-1D$  and  $+2D$  indicate a prominent alternating reattachment, while the cross sections at  $0D$  and  $+1D$  indicate a more continuous, steady reattachment. This highlights the presence of spanwise variability during the alternating reattachment, i.e., some sections of the span might be alternating while some might be more steadily reattaching. Moreover, modes at cross sections of  $-1D$  and  $+2D$  are negatively correlated on average (correlation between the median filtered lift coefficients is  $-0.54$ ), i.e., when mode 1 is seen at  $-1D$ , mode 2 is seen at  $2D$  on the cylinder on average. This, along with the more continuous reattachment at  $0D$  and  $+1D$ ,

indicates the presence of spanwise cells of different reattachment configurations in alternating reattachment. The length and position of cells appear to be highly sensitive to the setup. Recently, Aasland *et al.* (2023) reported the existence of spanwise cellular structures in the reattachment regime  $L^* = 3$  at  $Re = 500$  and emphasized their unpredictability.

A consequence of sensitive spanwise coherence is that different measurement techniques like cross-sectional pressure measurements, load measurements on either a section or the entirety of the cylinder could result in different  $C_L$  measurements. This could also contribute toward the difference between the current fluctuating coefficients and those of Alam *et al.* (2003) and Alam (2014) in the reattachment regime (in addition to the difference in surface roughness and Reynolds numbers between the investigations).

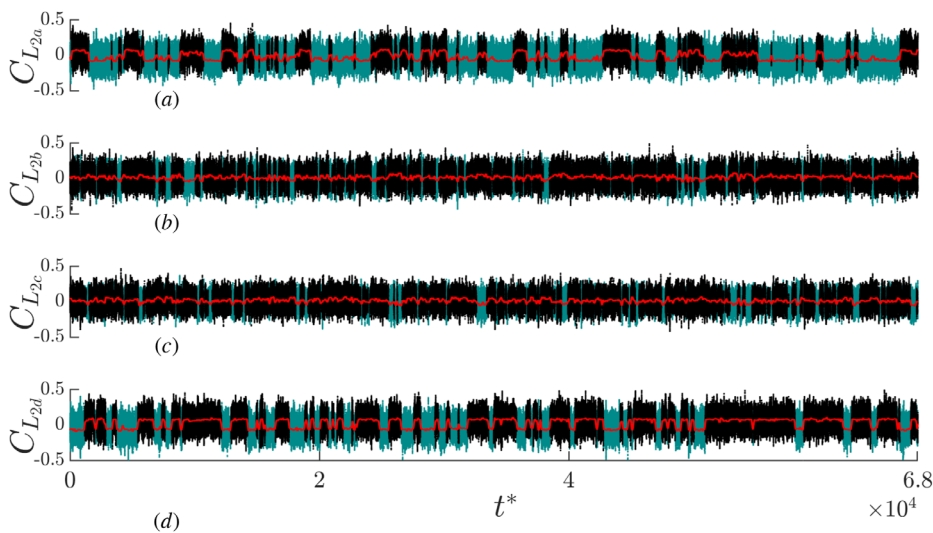


**FIG. 23.** Time history of the lift coefficients on the downstream cylinder at different spanwise measurement planes at a pitch ratio of  $L^* = 1.75$  and  $Re \approx 3 \times 10^5$ . (a)  $-1D$ , (b)  $0D$ , (c)  $+1D$ , and (d)  $+2D$ , where  $0D$  is the midspan. Cyan line: mode 1, black line: mode 2. Red line: Moving median of 100 convective cycles.

**G. The influence of Reynolds number**

**1. Mean coefficients of drag and lift**

Figure 24 gives the variation of the mean coefficient of drag of the two cylinders with pitch ratio for different postcritical Reynolds numbers. For the upstream cylinder,  $C_{D1}$  increases with increasing Reynolds number for  $L^* > L_c^*$ . This increase in  $C_{D1}$  is similar in proportion to that seen for an isolated cylinder for the same increase in Reynolds number. For example, at  $L^* = 4$ ,  $C_{D1}$  increases by  $\sim 9\%$  when the Reynolds number is increased from  $3 \times 10^5$  to  $6 \times 10^5$ , and the corresponding increase in the coefficient of drag for an isolated cylinder is  $\sim 9.5\%$ . The mean drag coefficient of the downstream cylinder,  $C_{D2}$ , does not show significant variation with Reynolds number. Beyond the critical pitch ratio,  $C_{D2}$  is approximately the same for all Reynolds numbers for a given  $L^*$ . When the downstream cylinder is well inside the reattachment regime ( $L^* \leq 2$ ),  $C_{D2}$  decreases slightly with increasing Reynolds number (thrust increases). At  $L^* = 3.25$ , the flow is bistable and  $C_{D1}$  increases for increasing Reynolds number. This indicates that for a fixed  $L^*$  in the bistable regime, the shear layer reattaches for a smaller duration as Reynolds number is increased.

**2. Fluctuating coefficients of drag and lift**

The variations of the fluctuating coefficients of drag and lift with pitch ratio at different Reynolds numbers are given in Fig. 25. Similar to the mean force coefficients, fluctuating coefficients of the upstream cylinder increase with an increase in Reynolds number in the co-shedding regime,  $L^* > L_c^*$ . This increase is in proportion to that seen for an isolated cylinder.

Current results indicate that both the mean and fluctuating drag coefficients of the downstream cylinder near  $L^* = 2.5$  increase when Reynolds number increases from  $3 \times 10^5$  to  $5 \times 10^5$  but decrease when it increases from  $5 \times 10^5$  to  $6 \times 10^5$ , thus forming a maximum at  $Re = 5 \times 10^5$ . Interestingly, the pitch ratio at which this peculiarity is seen currently coincides with the pitch ratio at which local peaks are

seen in the fluctuating and mean force coefficients in the study by Alam et al. (2003).

Alam et al. (2003) reported alternating reattachment over  $1 < L^* < 3$ , steady reattachment over  $3 < L^* < 4$ , and a maximum in the fluctuations of force were observed at  $L^* = 2.4$ . In the current investigation, alternating reattachment is observed over  $1.5 \leq L^* < 2.25$ , continuous reattachment over  $2.25 < L^* \leq 3$ , and the maximum is at  $L^* = 2.5$ . The similarity between the two results is that the peak in fluctuating force coefficients is found near the transition from the alternating reattachment to the steady reattachment.

Alam et al. (2003) and Alam (2014) also found a local minimum in the reattachment angle at  $L^* = 2.4$  for  $Re = 6.5 \times 10^4$ , leading to the proposal of a different reattachment configuration to explain the minimum in reattachment and the corresponding maxima in the fluctuating forces. The new reattachment configuration is hypothesized to be linked to the transition to turbulence in the shear layer post separation from the upstream cylinder and is hence sensitive to the Reynolds number and pitch ratio. The current investigation focuses on postcritical Reynolds numbers and thus the boundary layer on the upstream cylinder is expected to be turbulent before separation.

Upon closer inspection of flow at  $4 \times 10^5 \leq Re \leq 5 \times 10^5$  in the current study, we found that a harmonic of the frequency of shedding is close to a structural frequency of the cylinder, thus resulting in a larger structural response due to resonance at these Reynolds numbers. That is, the downstream cylinder was noticeably vibrating in the range of  $2.2 \leq L^* \leq 2.75$  for  $4 \times 10^5 \leq Re \leq 5 \times 10^5$ , and results, particularly of fluctuating components in this range, should be viewed with caution. From Fig. 22, it is clear that the spanwise correlation of the lift increases with an increase in pitch ratio in the reattachment regime even for  $Re \approx 3 \times 10^5$  (where no prominent flow–structure resonance was observed). This indicates that the downstream cylinder is more susceptible to resonance in the continuous reattachment regime since the magnitude of force fluctuations on the downstream cylinder is larger due to an increase in spanwise coherence.

To summarize, Alam et al. (2003) and Alam (2014) reported prominent peaks in  $\sigma_{C_D}$  and  $\sigma_{C_L}$  at  $L^* = 2.4$  for  $Re = 3.2 \times 10^4$  and

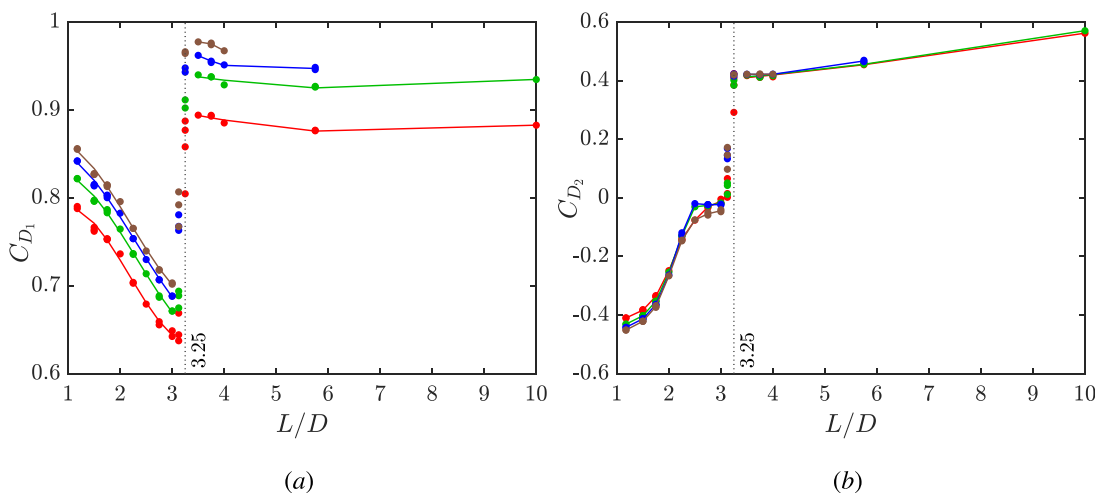


**FIG. 24.** Influence of Reynolds number on the mean drag coefficient of (a) the upstream cylinder and (b) the downstream cylinder at different pitch ratios. Red-filled circle:  $Re \approx 3 \times 10^5$ , green-filled circle:  $Re \approx 4 \times 10^5$ , blue-filled circle:  $Re \approx 5 \times 10^5$ , and brown-filled circle:  $Re \approx 6 \times 10^5$ .

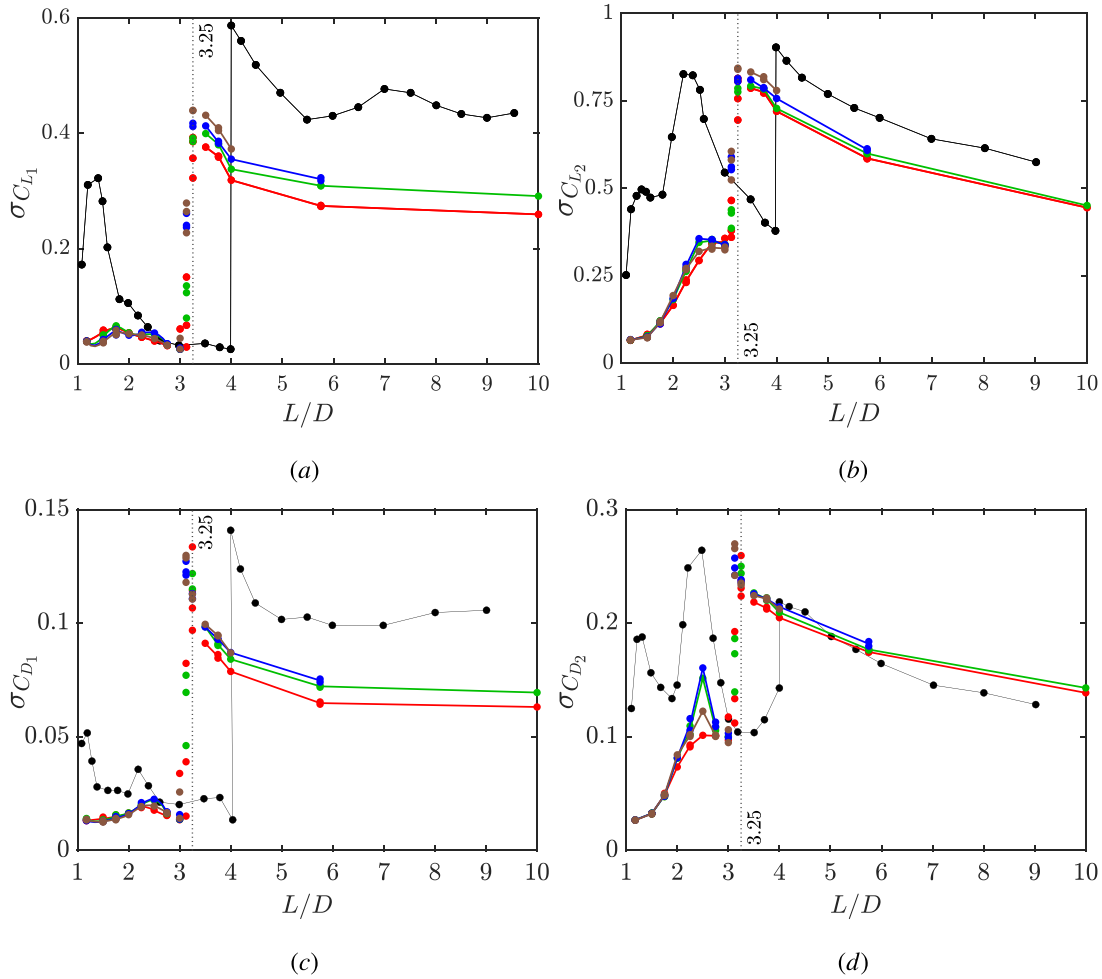


**FIG. 25.** The variation of fluctuating force coefficients with pitch ratio. (a) and (b) Fluctuating lift coefficient, (c) and (d) fluctuating drag coefficient, (a) and (c) upstream cylinder, and (b) and (d) downstream cylinder. —: Alam *et al.* (2003),  $Re = 6.5 \times 10^4$ , red line: current,  $Re \approx 3 \times 10^5$ ; green line: current,  $Re \approx 4 \times 10^5$ ; blue line: current,  $Re \approx 5 \times 10^5$ ; and brown line: current,  $Re \approx 6 \times 10^5$ .

$Re = 6.5 \times 10^4$ . Current results at  $Re = 3 \times 10^5$  do not contain this maximum. However, evidence indicates that the continuous reattachment regime is more coherent across the span than the alternating reattachment regime. This increase in coherence could result in large structural response and hence large increases in  $\sigma_{C_D}$  and  $\sigma_{C_L}$  at specific Reynolds numbers in this range of pitch ratios.

#### IV. CONCLUSIONS

*Postcritical flow over inline rough cylinders*, which is of great relevance to engineered structures, has not been well explored. It is in this scenario that we have quantified the forces on two inline cylinders and the corresponding shedding frequencies for various pitch ratios, both of which are crucial to the fluid–structure interaction. From the objectives originally discussed in the introductory section, the following conclusions have been found through this investigation:

1. On the influence of Reynolds number on the force coefficients and the critical pitch ratio in the postcritical regime:

- (a) Our results reveal that while the flow configurations and the broad trends in the Strouhal number remain similar, the boundaries of these configurations are different from their subcritical counterparts. The critical pitch ratio,  $L_c^* = 3.25$ , falls at the lower end of the previously reported lower Reynolds number values of  $3 \leq L_c^* \leq 5$  (Summer, 2010; Alam and Zhou, 2007). This reduction implies that structures designed with pitch ratios in the range  $3 < L^* < 5$  could experience much larger drag coefficients if the Reynolds number or surface roughness is increased (i.e. shifting the flow regime to postcritical).
- (b) At a postcritical  $Re \approx 3 \times 10^5$ , as the pitch ratio is decreased from 10, the mean coefficient of drag on the upstream cylinder,  $C_{D1}$ , remains constant at  $\approx 0.88$  down to  $L^* \approx 4$ . Below this it slightly increases, indicating a wider wake. The Strouhal number also decreases with pitch ratio between  $L_c^* \leq L^* \leq 4$ .  $C_{D1}$  then drops steeply to  $\approx 0.6$  near the critical pitch ratio of  $L_c^*$  and then increases

- with further decreases in  $L^*$ . At the closest pitch ratio tested (1.175),  $C_{D_1} \approx 0.78$ .
- (c)  $C_D$  of an isolated cylinder of the same surface roughness is 0.88 at  $Re \approx 3 \times 10^5$ . At  $L^* = 10$ ,  $C_{D_2}$  ( $C_D$  of the downstream cylinder) is  $\approx 63\%$  of that seen on an isolated cylinder.  $C_{D_2}$  decreases slightly with decreasing pitch ratio from  $L^* = 10$  to 4. A comparison of the circumferential pressure distributions indicates that this decrease is likely due to the difference between the velocity and the pressure used for normalization and those effectively operating on the downstream cylinder.
  - (d) In the postcritical regime, the mean drag coefficient of the upstream cylinder increases with an increase in Reynolds number. Furthermore, the magnitude of the increase is similar to the corresponding increase seen for an isolated cylinder at all pitch ratios, except near the critical pitch ratio, indicating that the influence of Reynolds number on the upstream cylinder is similar regardless of the presence of the downstream cylinder. On the other hand, the mean drag coefficient of the downstream cylinder shows little variation across the Reynolds numbers tested, except for a slight decrease with Reynolds number at the closest pitch ratios (i.e.,  $L^* \leq 2$ ). In addition, the mean drag coefficients of the downstream cylinder from the current and previous investigations (Alam *et al.*, 2003; Okajima, 1979; and Dubois and Andrianne, 2022) are remarkably close despite large differences in the Reynolds number and surface roughness.
  - (e) Comparing separation angle on the downstream cylinder across various investigations, Aasland *et al.* (2022) predicted that the inflow Reynolds number might have limited influence on the flow over the downstream cylinder in the subcritical regime. Furthermore, it was proposed that flow over the downstream cylinder could be determined using pitch ratio as the single governing parameter. Current results extend this strong agreement in the mean drag coefficient of the downstream cylinder to postcritical Reynolds numbers. In addition, an increase in surface roughness also appears to have only a minor influence (if any) on the mean drag coefficient of downstream cylinder. However, the fluctuations in drag and lift of both the cylinders observed in this investigation are different from those reported on smooth cylinders in subcritical flows.
2. Table II provides a graphical summary bringing together our observations and describing the variation in postcritical flow. Further conclusions are as follows:
- (a) The upstream shear layers reattach continuously on the downstream cylinder for  $2.25 < L^* \leq 3$ , and alternately for  $1.5 \leq L^* < 2.25$ . As the downstream cylinder is moved closer, transition to alternating reattachment is seen when the pressure fluctuations in the impinging shear layers from the upstream cylinder are of the same magnitude as those caused due to separation on the downstream cylinder. This transition also correlates with the pitch ratio where K-H frequencies disappear along with an appearance of the second harmonic of the shedding in the spectra of pressure fluctuations.
  - (b) During alternating reattachment, the boundary layer on one half ( $0^\circ \leq \theta \leq 180^\circ$ ) of the upstream cylinder undergoes earlier separation and the corresponding half on the downstream cylinder experiences later reattachment than the other half ( $180^\circ \leq \theta \leq 360^\circ$ ). When later reattachment occurs, the flow separation point on the downstream cylinder becomes less distinct. Spectra of pressure fluctuations and the circumferential distribution of fluctuating pressure ( $\sigma_{C_p}$ ) indicate that a zone of more distinct rolled-up vorticity of a larger length scale exists in the half of later reattachment in agreement with the observations of Lin *et al.* (2002) and Aasland *et al.* (2023). Current results reveal that this causes an alternating cross-sectional lift on the two cylinders, i.e., on the upstream cylinder, lift acts in the opposite direction to the half that undergoes earlier separation while on the downstream cylinder, lift acts in the direction of that half (see Fig. 17).
  - (c) The spectra of the fluctuations in surface pressure on the downstream cylinder indicate that its presence stabilizes the shear layers emanating from the upstream cylinder and delays the onset or partially suppresses the growth of Kelvin–Helmholtz instabilities. Aasland *et al.* (2022) also found a delayed onset of K–H oscillations in the shear layers emanating from the upstream cylinder for smooth tandem cylinders at  $Re = 10^4$ .
3. On the dynamics of force coefficients in the postcritical regime:
- (a) No prominent maxima in  $\sigma_{C_D}$  or  $\sigma_{C_L}$  are seen within the reattachment regime in the current investigation at  $Re \approx 3 \times 10^5$ . At  $Re = 3.2 \times 10^4$  and  $6.5 \times 10^4$ , Alam *et al.* (2003) and Alam (2014) found prominent peaks in  $\sigma_{C_D}$  and  $\sigma_{C_L}$  of the downstream cylinder at  $L^* = 2.4$  and the prominence of the peaks increased with increase in the Reynolds number from  $9.7 \times 10^3$  to  $6.5 \times 10^4$ . Alam (2014) proposed that some pitch ratios in a specific range of Reynolds numbers result in a different flow configuration due to variation in the location of transition to turbulence in the separated shear layers of the upstream cylinder. Since the incoming Reynolds number is postcritical in the current investigation, boundary layers on the upstream cylinder are turbulent before separation at all pitch ratios. Thus, the current results of  $\sigma_{C_D}$  or  $\sigma_{C_L}$  do not contain prominent maxima in the reattachment regime.
  - (b) In addition, the current results reveal that the larger pitch ratios in the reattachment regime are more susceptible to structural resonance of the downstream cylinder due to an increased spanwise correlation in both lift and drag forces. This increased structural response could also lead to localized increases in  $\sigma_{C_D}$  and  $\sigma_{C_L}$  at specific Reynolds numbers in this range of pitch ratios.
4. On the spanwise variation of the flow in the bistable and the reattachment regime:
- (a) In the bistable regime, either the reattachment flow or the co-shedding flow exists at both the measurement locations (separated by two diameters in the spanwise direction). Moreover, transitions between the two occur simultaneously. Thus, it is likely that a given flow pattern exists across span in the bistable regime.

- (b) In the alternating reattachment regime, the half of the “earlier separation” alternates across sections of the cylinder span. Similar spanwise structures have been reported previously in the study by [Lin et al. \(2002\)](#) and [Aasland et al. \(2023; 2022\)](#), albeit at considerably lower Reynolds numbers. These flow structures are highly sensitive to the geometry of the setup. This suggests that  $C_L$  estimated through integrating sectional pressures could be different from that directly measured on a length of the cylinder.

## ACKNOWLEDGMENTS

This research was supported by the Australian Government through the Australian Research Council’s Linkage Projects funding scheme (No. LP180100234).

## AUTHOR DECLARATIONS

### Conflict of Interest

The authors have no conflicts to disclose.

### Author Contributions

**Anil Pasam:** Conceptualization (equal); Data curation (lead); Formal analysis (lead); Investigation (lead); Methodology (equal); Validation (equal); Visualization (lead); Writing – original draft (lead); Writing – review & editing (supporting). **Daniel Tudball Smith:** Conceptualization (equal); Data curation (supporting); Formal analysis (supporting); Investigation (supporting); Methodology (equal); Project administration (equal); Supervision (supporting); Validation (equal); Writing – review & editing (supporting). **David Burton:** Conceptualization (equal); Data curation (supporting); Formal analysis (supporting); Funding acquisition (equal); Project administration (equal); Resources (equal); Software (equal); Supervision (lead); Validation (equal); Writing – review & editing (supporting). **Mark C. Thompson:** Conceptualization (equal); Data curation (supporting); Formal analysis (supporting); Funding acquisition (equal); Project administration (equal); Resources (equal); Supervision (lead); Validation (equal); Writing – review & editing (lead).

## DATA AVAILABILITY

The data that support the findings of this study are available from the corresponding author upon reasonable request.

## REFERENCES

- Aasland, T. E., Pettersen, B., Andersson, H. I., and Jiang, F., “Revisiting the reattachment regime: A closer look at tandem cylinder flow at  $re = 10^4$ ,” *J. Fluid Mech.* **953**, A18 (2022).
- Aasland, T. E., Pettersen, B., Andersson, H. I., and Jiang, F., “Asymmetric cellular instability in the gap between tandem cylinders,” *J. Fluid Mech.* **966**, A39 (2023).
- Achenbach, E., “Influence of surface roughness on the cross-flow around a circular cylinder,” *J. Fluid Mech.* **46**, 321–335 (1971).
- Achenbach, E. and Heinecke, E., “On vortex shedding from smooth and rough cylinders in the range of Reynolds numbers  $6 \times 10^3$  to  $5 \times 10^6$ ,” *J. Fluid Mech.* **109**, 239–251 (1981).
- Alam, M. M., “The aerodynamics of a cylinder submerged in the wake of another,” *J. Fluids Struct.* **51**, 393–400 (2014).
- Alam, M. M., Moriya, M., Takai, K., and Sakamoto, H., “Fluctuating fluid forces acting on two circular cylinders in a tandem arrangement at a subcritical Reynolds number,” *J. Wind Eng. Ind. Aerodyn.* **91**, 139–154 (2003).
- Alam, M. M. and Zhou, Y., “Phase lag between vortex sheddings from two tandem bluff bodies,” *J. Fluids Struct.* **23**, 339–347 (2007).
- Alam, M. M. and Zhou, Y., “Strouhal numbers, forces and flow structures around two tandem cylinders of different diameters,” *J. Fluids Struct.* **24**, 505–526 (2008).
- Allen, H. J. and Vincenti, W. G., “Wall interference in a two-dimensional-flow wind tunnel, with consideration for the effect of compressibility,” Report No. NACA-WR-A-63 (1944).
- Bergh, H. and Tijdeman, H., *Theoretical and Experimental Results for the Dynamic Response of Pressure Measuring Systems* (National Lucht- en Ruimtevaartlaboratorium, 1965).
- Carmo, B. S., Meneghini, J. R., and Sherwin, S. J., “Secondary instabilities in the flow around two circular cylinders in tandem,” *J. Fluid Mech.* **644**, 395–431 (2010).
- Cheung, “Effect of turbulence on the aerodynamics and response at a circular structure in wind blow,” Doctorate thesis (Monash University, 1983).
- Dubois, R. and Andrienne, T., “Flow around tandem rough cylinders: Effects of spacing and flow regimes,” *J. Fluids Struct.* **109**, 103465 (2022).
- Farell, C., Carrasquel, S., Güven, O., and Patel, V. C., “Effect of wind-tunnel walls on the flow past circular cylinders and cooling tower models,” *J. Fluids Eng.* **99**, 470–479 (1977).
- Gu, Z., Sun, T., He, D. X., and Liang, L. Z., “Two circular cylinders in high-turbulence flow at supercritical Reynolds number,” *J. Wind Eng. Ind. Aerodyn.* **49**, 379–388 (1993).
- Güven, O., Farell, C., and Patel, V. C., “Surface-roughness effects on the mean flow past circular cylinders,” *J. Fluid Mech.* **98**, 673–701 (1980).
- Igarashi, T., “Characteristics of the flow around two circular cylinders arranged in tandem: 1st report,” *Bull. JSME* **24**, 323–331 (1981).
- Igarashi, T., “Characteristics of the flow around two circular cylinders arranged in tandem: 2nd Report, unique phenomenon at small spacing,” *Bull. JSME* **27**, 2380–2387 (1984).
- Lin, J. C., Yang, Y., and Rockwell, D., “Flow past two cylinders in tandem: Instantaneous and averaged flow structure,” *J. Fluids Struct.* **16**, 1059–1071 (2002).
- Ljungkrona, L., Norberg, C., and Sundén, B., “Free-stream turbulence and tube spacing effects on surface pressure fluctuations for two tubes in an in-line arrangement,” *J. Fluids Struct.* **5**, 701–727 (1991).
- Nikurdase, J., *Stromungsgesetze in rauhen rohren* (Forschungsheft, Germany, 1933).
- Okajima, A., “Flows around two tandem circular cylinders at very high Reynolds numbers,” *JSME Int. J. Ser. B/Fluids Therm. Eng.* **22**, 504–511 (1979).
- Okajima, A. and Sugitani, K., “Flow around a circular cylinder immersed in a wake of an identical cylinder (drag coefficient and Strouhal number),” *Trans. JSME B* **50**, 2531–2538 (1984).
- Pasam, A., Smith, T. D., Holmes, J. D., Burton, D., and Thompson, M. C., “The influence of surface roughness on postcritical flow over circular cylinders revisited,” *J. Fluid Mech.* **975**, A36 (2023).
- Roshko, A., “Experiments on the flow past a circular cylinder at very high Reynolds number,” *J. Fluid Mech.* **10**, 345–356 (1961).
- Schewe, G., van Hinsberg, N. P., and Jacobs, M., “Investigation of the steady and unsteady forces acting on a pair of circular cylinders in crossflow up to ultrahigh Reynolds numbers,” *Exp. Fluids* **62**, 1–18 (2021).
- Schewe, G. and Jacobs, M., “Experiments on the flow around two tandem circular cylinders from sub-up to transcritical Reynolds numbers,” *J. Fluids Struct.* **88**, 148–166 (2019).
- Speidel, L., “Einfluß der oberflächenrauigkeit auf die strömungsverluste in ebenen schaufelgittern,” *Forsch. Ing-Wes.* **20**, 129–140 (1954).
- Summer, D., “Two circular cylinders in cross-flow: A review,” *J. Fluids Struct.* **26**, 849–899 (2010).
- van Hinsberg, N. P., “The Reynolds number dependency of the steady and unsteady loading on a slightly rough circular cylinder: From subcritical up to high transcritical flow state,” *J. Fluids Struct.* **55**, 526–539 (2015).
- Xu, G. and Zhou, Y., “Strouhal numbers in the wake of two inline cylinders,” *Exp. Fluids* **37**, 248–256 (2004).
- Zdravkovich, M. M., “Aerodynamics of two parallel circular cylinders of finite height at simulated high Reynolds numbers,” *J. Wind Eng. Ind. Aerodyn.* **6**, 59–71 (1980).
- Zdravkovich, M. M., “Review of flow interference between two circular cylinders in various arrangements,” *J. Fluids Eng.* **99**, 618–633 (1977).



- Zdravkovich, M. M., "The effects of interference between circular cylinders in cross flow," *J. Fluids Struct.* **1**, 239–261 (1987).
- Zdravkovich, M. M. and Pridden, D. L., "Interference between two circular cylinders; Series of unexpected discontinuities," *J. Wind Eng. Ind. Aerodyn.* **2**, 255–270 (1977).
- Zhang, H. and Melbourne, W. H., "Interference between two circular cylinders in tandem in turbulent flow," *J. Wind Eng. Ind. Aerodyn.* **41**, 589–600 (1992).
- Zhou, Q., Alam, M. M., Cao, S., Liao, H., and Li, M., "Numerical study of wake and aerodynamic forces on two tandem circular cylinders at  $Re = 10^3$ ," *Phys. Fluids* **31**, 045103 (2019).
- Zhou, Y. and Alam, M. M., "Wake of two interacting circular cylinders: A review," *Int. J. Heat Fluid Flow* **62**, 510–537 (2016).
- Zhou, Y. and Yiu, M. W., "Flow structure, momentum and heat transport in a two-tandem-cylinder wake," *J. Fluid Mech.* **548**, 17–48 (2006).